Monoacylglycerol lipase inhibitors reverse paclitaxel-induced nociceptive behavior and proinflammatory markers in a mouse model of chemotherapy-induced neuropathy*

Zachary A Curry, Jenny L Wilkerson, Deniz Bagdas, S Lauren Kyte, Nipa Patel, Giulia Donvito, Mohammed A Mustafa, Justin L Poklis, Micah J Niphakis, Ku-Lung Hsu, Benjamin F Cravatt, David A Gewirtz, M Imad Damaj, Aron H Lichtman

Affiliations:

Department of Pharmacology and Toxicology, Virginia Commonwealth University, Richmond, VA, USA (ZAC, JLW, DB, MAM, SLK, NP, GD, JLP, DAG, MID, AHL)

The Skaggs Institute for Chemical Biology and Department of Chemical Physiology, The Scripps Research Institute, La Jolla, CA, USA (MJN, BFC)

Department of Chemistry, University of Virginia, Charlottesville, VA, USA (KLH)

1

a) A running title: MAGL inhibitors attenuate paclitaxel-induced allodynia

b) Corresponding Author:
Aron H. Lichtman

P.O. Box 980613
Dept. of Pharmacology & Toxicology
Virginia Commonwealth University
Richmond, VA 23298-0613

Email: aron.lichtman@vcuhealth.org

Phone: +1(804) 628-2495

Fax: +1(804) 827-0377

c) The number of text pages, number of tables, figures, and references, and the number of words in the Abstract, Introduction, and Discussion:

Number of text pages: 19
Number of figures: 13; Supplemental figures: 4
Number of references: 66
Number of words in Abstract: 248
Number of words in Introduction: 748
Number of words in Discussion: 1,467

d) List of nonstandard abbreviations:
2-AG, 2-arachidonoylglycerol; ABHD6, alpha beta hydrolase domain-containing protein 6; ANOVA, analysis of variance; CIPN, Chemotherapy-induced peripheral neuropathy; CNS, central nervous system; CPP, conditioned place preference; DRG, dorsal root ganglia; MAGL, monoacylglycerol lipase; MCP-1, monocyte chemoattractant protein-1; NSCLC, non-small cell lung cancer; PBS, phosphate buffered saline

e) Assignment Guide:
Behavioral Pharmacology

Drug Discovery and Translational Medicine

Neuropharmacology

Abstract

Although paclitaxel effectively treats various cancers, its debilitating peripheral neuropathic pain side effects often persist long after treatment has ended. Therefore, a compelling need exists for the identification of novel pharmacologic strategies to mitigate this condition. As inhibitors of monoacylglycerol lipase (MAGL), the primary hydrolytic enzyme of the endogenous cannabinoid 2-arachidonyolglycerol, produce antinociceptive effects in numerous rodent models of pain, we investigated whether inhibitors of this enzyme (i.e., JZL184 and MJN110) would reverse paclitaxel-induced mechanical allodynia in mice. These drugs dose-dependently reversed allodynia with respective ED_{50} values (95% C.L.) of 8.4 (5.2-13.6) and 1.8 (1.0-3.3) mg/kg. Complementary genetic and pharmacologic approaches revealed that the anti-allodynic effects of each drug require both cannabinoid receptors, CB_1 and CB_2. MJN110 reduced paclitaxel-mediated increased expression of monocyte chemoattractant protein-1 (MCP-1, CCL2) and phospho-p38 MAPK in dorsal root ganglia as well as MCP-1 in spinal dorsal horn. Whereas the antinociceptive effects of high dose JZL184 (40 mg/kg) underwent tolerance following six days of repeated dosing, repeated administration of a threshold dose (i.e., 4 mg/kg) completely reversed paclitaxel-induced allodynia. In addition, we found that the administration of MJN110 to control mice lacked intrinsic rewarding effects in the conditioned place preference (CPP) paradigm. However, it produced a CPP in paclitaxel-treated animals, suggesting a reduced paclitaxel-induced aversive state. Importantly, JZL184 did not alter the antiproliferative and apoptotic effects of paclitaxel in A549 and H460 non-small cell lung cancer cells. Taken together, these data indicate that MAGL inhibitors reverse paclitaxel-induced neuropathic pain without interfering with chemotherapeutic efficacy.

Introduction

  Paclitaxel is a widely prescribed chemotherapeutic for the treatment of breast, lung and other cancers, but causes a variety of serious side effects, including peripheral neuropathy, leukopenia, joint or muscle pain, vomiting, and alopecia (Ghersi *et al.*, 2015). Chemotherapy-induced peripheral neuropathy (CIPN) causes severe sensory disturbances that range from mild tingling to spontaneous painful burning paresthesia affecting the longest sensory nerves to the hands and feet (Dougherty *et al.*, 2004) and can persist long after treatment cessation (Tanabe *et al.*, 2013) in up to 68% of chemotherapy cancer patients (Seretny *et al.*, 2014). As traditional analgesics generally lack efficacy in treating this condition (Kim *et al.*, 2015), a pressing need exists for novel analgesic strategies. However, the endogenous cannabinoid system contains several potential targets of promise to treat CIPN. Here, we employ a mouse paclitaxel model of CIPN to explore whether inhibition of monoacylglycerol lipase (MAGL) (Dinh *et al.*, 2002), the primary hydrolytic enzyme of the endogenous cannabinoid 2-arachidonoylglycerol (2-AG) (Mechoulam *et al.*, 1995; Sugiura *et al.*, 1995; Blankman *et al.*, 2007), will reduce nociceptive behavior and associated inflammatory responses.

  MAGL inhibitors increase 2-AG, decrease arachidonic acid levels in the CNS (Long *et al.*, 2009), and produce anti-allodynic effects in rodent neuropathic pain models, including chronic constriction injury of the sciatic nerve (Ignatowska-Jankowska *et al.*, 2015; Wilkerson *et al.*, 2016b; Crowe *et al.*, 2017) and cisplatin neuropathy (Guindon *et al.*, 2013). Importantly, the CB_2 receptor agonist AM1710 (Deng *et al.*, 2015b) and the MAGL inhibitor JZL184 (Slivicki *et al.*, 2017) reverse paclitaxel-induced allodynia in mice. In the present study, we build upon this work using the MAGL inhibitors JZL184 (Long *et al.*, 2009a) and MJN110 (Niphakis *et al.*, 2013) in the paclitaxel mouse model of CIPN. Although MJN110 is more potent than JZL184 (Ignatowska-Jankowska *et al.*, 2015), it also inhibits α/β-hydrolase domain 6 (ABHD6) (Niphakis *et al.*, 2013), which metabolizes a much smaller percentage of 2-AG than MAGL (Blankman *et al.*, 2007). To control for this off-target effect, we tested the selective ABHD6 inhibitor KT195 (Hsu *et al.*, 2012; Wilkerson *et al.*, 2016a). We used complementary genetic and pharmacologic approaches to assess the contribution of CB_1 and CB_2 receptors to observed pharmacological effects of the inhibitors. Because CIPN persists in patients long after chemotherapy treatment, we explored whether the antinociceptive effects of JZL184 would undergo tolerance or be maintained after repeated administration. We also explore whether repeated administration of JZL184 increases endocannabinoid levels and decreases arachidonic acid levels, along with prostaglandin D2 (PGD_2) (Nomura *et al.*, 2011), in the lumbar spinal cord of paclitaxel-treated mice.

In addition to neurotoxicity (Bobylev *et al.*, 2015), paclitaxel causes inflammation within the dorsal root ganglia (DRG) and activates toll-like receptor 4 (Li *et al.*, 2014) with subsequent p38 MAPK expression and activation through phosphorylation, increasing phosphorylated p38 MAPK (phospho-p38) (Li *et al.*, 2015). Paclitaxel also increases the chemokine monocyte chemoattractant protein-1 (MCP-1)/(C-C motif) ligand 2 (CCL2) expression in the DRG (Zhang *et al.*, 2013; Makker *et al.*, 2017) and the spinal cord (Pevida *et al.*, 2013; Zhang *et al.*, 2013), causing sensory neuron sensitization through transient receptor potential channel activation (Jung *et al.*, 2008) and increased intracellular calcium (Zhang *et al.*, 2013). Antibodies targeting MCP-1 reverse paclitaxel allodynia (Zhang *et al.*, 2016). In contrast, inhibition of phospho-p38 does not reverse, but prevents (Li *et al.*, 2015) allodynia development. Although a CB_2 receptor agonist inhibits spinal MCP-1 expression associated with paclitaxel (Deng *et al.*, 2015), MAGL inhibitors remain unexplored. Accordingly, we tested whether MAGL inhibition would ameliorate paclitaxel-induced expression of MCP-1 and phospho-p38 in the DRG and spinal dorsal horn.

Along with mechanical allodynia, we assessed whether MJN110 produces a conditioned place preference (CPP) in paclitaxel-treated mice. The CPP paradigm allows for disassociation of a drug's analgesic profile and its intrinsic rewarding effects, as shown for cisplatin neuropathy (Park *et al.*, 2013; Krukowski *et al.*, 2017) and osteoarthritis (Havelin *et al.*, 2016). However, CPP has not been used in paclitaxel-induced CIPN to examine MAGL inhibitors. Here, we test whether MJN110 produces a CPP in paclitaxel-treated mice, indicating relief from an aversive state not observed in control mice.

Lastly, as paclitaxel-induced CIPN develops during chemotherapy treatment, it is important to test whether candidate antinociceptive agents, such as MAGL inhibitors, interfere with paclitaxel's anti-tumor effects. Thus, we examined whether JZL184 affects the anti-proliferative and apoptotic activity of paclitaxel in the human cell lines of non-small cell lung cancer (NSCLC) (Ettinger and Akerley, 2010) A549 (Marostica *et al.*, 2015) and H460 (Huisman *et al.*, 2002) cells.

Materials and Methods

Animals

Adult male C57BL/6J mice with starting weights of 24.8 ± 0.16 grams (Jackson Laboratories, Bar Harbor, ME) were used in all studies except in experiments employing CB_1 (-/-) and CB_2 (-/-) mice. Male and female CB_1 (-/-) (Zimmer *et al.*, 1999) and CB_2 (-/-) (Jackson Laboratories, Bar Harbor, ME) and matched wild-type control mice were received from the Virginia Commonwealth University (VCU) Massey Cancer Center Transgenic/Knockout Mouse Shared Resource. Both lines of transgenic mice have been backcrossed with C57BL/6J mice. Based on genotyping analysis, CB_1 (-/-) mice were 90% similar to C57BL/6J, 6% similar to C57BL/6N and 4% similar to 129/Sv mice. CB_2 (-/-) mice were 71% similar to C57BL/6J and 27% similar to C57BL/6N and 2% similar to 129/Sv mice. Animals were housed 4 per cage, with separation as needed when fighting, and maintained in the AAALAC-approved vivarium at Virginia Commonwealth University. Animals were provided with water and Teklad LM-485 Mouse Diet (7012; Envigo/Teklad Diets, Madison, WI) chow *ad libitum* with a 12-hour light/dark cycle beginning at 0600 h. Animal studies were conducted in compliance with the National Institutes of Health Guide for the Care and Use of Laboratory Animals and approved by the VCU Institutional Animal Care and Use Committee. During studies involving transgenic mice and pharmacologic antagonists (rimonabant or SR144528), the vivarium at VCU was undergoing renovation. Thus, mice were moved between vivarium rooms and exposed to construction noise. For all other studies, mice were housed undisturbed in the vivarium. Following behavioral testing, animals were euthanized using CO_2 asphyxiation and cervical dislocation unless tissue collection was performed. Tissue collection was performed after either rapid decapitation or isoflurane anesthesia.

Assessment of Mechanical Allodynia

Mice received a minimum of four days prior to experimentation to acclimate to the vivarium. Prior to behavioral assessment, mice were acclimated to the von Frey mesh elevated platform for a minimum of 40 min per day for a minimum of three days. During acclimation and testing, each mouse was placed in a ventilated Plexiglas cylinder, approximately 3 inches in diameter, minimizing locomotor activity. To assess paw withdrawal thresholds, von Frey filaments (North Coast Medical, Gilroy, CA) were applied to the hind paw for 3 s on each of three trials until a positive response was noted as a paw withdrawal to the stimulus. Testing began at the 0.6 g filament and moved sequentially to higher values (1, 1.4, 2, 4 g) until 5 out of 6 withdrawals were recorded. If a response occurred at 0.6 g, the 0.4, 0.16, and 0.07 g filaments were sequentially applied until five of six positive responses were obtained. A sixth

test was not conducted if the first five tests were positive. A maximum of 4 g was used to prevent sensitization. Results for each animal are reported as the average of both hind paws.

Drugs and Dosing

Paclitaxel (Taxol; Tocris Bioscience, Bristol, UK) was dissolved in a vehicle solution containing a 1:1:18 ratio of ethanol, emulphor-620 (Rhodia, Cranbury, NJ), and saline (0.9 % NaCl). A cycle of paclitaxel consisted of a total of four intraperitoneal (i.p.) injections of paclitaxel (8 mg/kg per injection) in which injections were given every other day (Toma *et al.*, 2017). Control (no paclitaxel) mice were given four injections of vehicle. The injection volumes were 0.01 ml per gram of body mass. The Cravatt laboratory at Scripps Research Institute, La Jolla, CA synthesized MJN110 and KT195 and the Drug Supply Program at the National Institute on Drug Abuse (Bethesda, MD) provided JZL184, rimonabant, and SR1445528. Doses of JZL184 (Long *et al.*, 2009a; Ghosh *et al.*, 2013; Ignatowska-Jankowska *et al.*, 2015), MJN110 (Niphakis *et al.*, 2013; Ignatowska-Jankowska *et al.*, 2015; Wilkerson, *et al.*, 2016b), and KT-195 (Hsu *et al.*, 2012; Wilkerson *et al.*, 2016a) were selected based on the results of previous *in vivo* and *in vitro* studies using these agents.

Following basal paw withdrawal assessment, paclitaxel or corresponding vehicle was administered as described above. Paclitaxel-treated and vehicle-pretreated control mice were separately housed to prevent cross-contamination. After confirmation of paw withdrawal thresholds, drugs were administered i.p. and mice were placed on the mesh for a minimum of 30 min prior to drug testing. Testing was conducted in a blinded manner with respect to acute drug treatment and a 72 h washout period was imposed between drug treatments as previously described (Ignatowska-Jankowska *et al.*, 2015; Wilkerson *et al.*, 2016a). All experiments were completed within eight weeks of the last paclitaxel/vehicle injection with a minimum five-day washout period before switching drugs. The same cohorts of CB_1 (-/-) and CB_2 (-/-) and (+/+) mice were used to test MJN110 and JZL184 within five weeks following paclitaxel cessation. A one-week washout period was used before switching drugs in these animals. For time course studies, testing began 0.5 h after drug administration and was finished 24 h post-treatment. Unless otherwise indicated, the antinociceptive effects of MJN110 were tested 3 h post-administration, while those of JZL184 was tested 2 h post-treatment. Rimonabant or SR144528 was administered 30 min prior to JZL184 or MJN110 (Wilkerson, *et al.*, 2016). Allodynia was confirmed prior to each test and persisted at eight weeks post-paclitaxel when testing was completed.

In the repeated JZL184 dosing experiment, C57BL/6J mice received a cycle of paclitaxel or vehicle and 10-12 days later received repeated i.p. injections of JZL184 or vehicle as previously

described (Kinsey *et al.*, 2013). Mice in the repeated JZL184 conditions received a daily i.p. injection of JZL184 (4 or 40 mg/kg) for six days. For the acute conditions, each mouse was given a daily i.p. injection of vehicle for five days and administered vehicle or JZL184 (4 mg/kg or 40 mg/kg) on day 6. All mice were tested for mechanical allodynia 2 h following the final injection on day 6.

Immunohistochemistry

Immunohistochemistry was conducted as previously described (Wilkerson *et al.*, 2012; Wilkerson *et al.*, 2016a) with slight modifications. Briefly, nine days after the cycle of paclitaxel or vehicle, mice were given an i.p. injection of MJN110 (5 mg/kg) or vehicle, and three hours later the mice were deeply anesthetized with isoflurane and perfused transcardially with saline followed by 4% paraformaldehyde in 0.1 M phosphate buffered saline (PBS), pH 7.4 (Thermo Fisher Scientific, Waltham, MA). Whole spinal columns were collected and fixed overnight in 4% paraformaldehyde at 4°C. Spinal columns then underwent EDTA decalcification (8% in PBS) for approximately 60 days and were sliced in 7 μm thick sections. DRG sections corresponding to the L5-L6 spinal cord were selectively examined. Tissue processing, paraffin embedding and slide preparation was provided by the Virginia Commonwealth University Cancer Mouse Models Core.

Samples were deparaffinized in Hemo De (Electron Microscopy Sciences, Hatfield, PA) and re-hydrated in 100% and 70% (v/v) ethanol (Pharmco-AAPER, Brookfield, CT) followed by PBS (Abcam, Cambridge, MA). Antigen retrieval was conducted in a pressure cooker (10 PSI) for 10 min in citrate buffer (2.1g/100mL deionized water, pH 6) followed by 10 min of cooling and 5 min in room-temperature PBS. Slides were blocked for 5-6 hours in 4.6% Normal Donkey Serum/PBS solution. Primary antibodies were applied in 0.5% bovine serum albumin/PBS solution with 1% sodium azide and incubated overnight at 4°C. The following primary antibodies were used: Rat anti-MCP-1 (1:50; ab8101; Abcam, Cambridge, MA) (Zoja *et al.*, 1997; Park *et al.*, 2011) and Rabbit anti-phospho-p38 MAPK (1:800; 4511S; Cell Signaling, Danvers, MA) (Wilkerson *et al.*, 2012; Shi *et al.*, 2017). On the following day, slides were incubated in secondary antibodies at room temperature. For MCP-1, rhodamine red donkey anti-rat (1:2000; 712-295-153; Jackson ImmunoResearch Laboratories, West Grove, PA) was used for two hours. For phospho-p38 MAPK, samples were incubated in biotinylated donkey anti-rabbit (1:1000 for DRG,1:1300 for dorsal horn; 711-065-152; Jackson ImmunoResearch Laboratories, West Grove, PA) for one hour, followed by processing with the Ultra-Sensitive ABC Peroxidase Standard Staining Kit (32050; ThermoFisher Scientific) and TSA Plus Cyanine 3 and Fluorescein System (PerkinElmer, Waltham, MA). Slides were then incubated in PBS, followed by a dip

in deionized water and coverslipped using Vectashield Antifade Mounting Medium with DAPI (H-1200; Vector Laboratories, Burlingame, CA). Imaging was done at 40x with a Zeiss AxioObserver A1 inverted microscope equipped with an Axiocam MRc5 color CCD camera and ZEN 2012 software (Carl Zeiss, AG) at the Virginia Commonwealth University Microscopy Facility. Images were converted to greyscale and underwent re-thresholding to reduce background fluorescence using Zeiss ZEN lite software (Carl Zeiss, AG) in a manner that was consistent across all treatment groups for each study. Spinal cord images were rotated or inverted as necessary for consistent orientation.

Densitometry analysis was conducted as previously described (Wilkerson *et al.*, 2012; Bagdas *et al.*, 2016; Wilkerson *et al.*, 2016a), according to the methods of (Samudio-Ruiz *et al.*, 2009; Zhang *et al.*, 2012). Densitometry analysis was conducted using Image J by selecting the anatomical location of the DRG or spinal dorsal horn in each image in an unbiased manner. For phospho-p38 MAPK analysis, four stained nuclei were selected at random from each image. Results are reported as the average of 4 separate sections per animal minus the average of four sections from a control slide lacking primary antibody. A sample size of four animals for each treatment condition was used.

For confocal microscopy and co-localization analysis, images were acquired at 63x using a Zeiss AxioObserver inverted LSM710 META confocal microscope and ZEN 2012. The entire z stack of a region was collected, and final images were generated from a single image along the z-plane.

Lipid Quantification

Quantification of endogenous cannabinoids was conducted as previously described (Ramesh *et al.*, 2011; Ignatowska-Jankowska *et al.*, 2015). Briefly, mice in the repeated administration study underwent mechanical allodynia testing and were euthanized by decapitation approximately 3-6 h after drug administration, a time point known to produce reliable elevations in 2-AG and decreased arachidonic acid (Long, *et al.*, 2009a). Spinal cord tissues were rapidly collected by hydraulic extrusion flushing the spinal canal with saline. The spinal cord was dissected to isolate the lumbar enlargement region (L4-L6), which was immediately frozen and stored at -80° C until further processing.

On the day of lipid extraction, the pre-weighed mouse samples were homogenized with 1.4 ml chloroform:methanol (containing 0.0348 g PMSF/ml), as previously described (Kinsey *et al.*, 2013). Six point calibration curves ranged from 0.078 pmol to 10 pmol for AEA, 0.125 nmol to 16 nmol for 2-AG, arachidonic acid and 1.75 pmol to 140 pmol PGD_2, a negative control, and blank control were prepared. ISTDs (50 µl of each of 1 pmol $AEA-d_8$, 1 nmol $2-AG-d_8$, 1 nmol arachidonic acid-d_8 and 14 pmol PGD_2-d_4) were added to each calibrator, control and sample, except the blank control. Each calibrator,

control and samples was then mixed with 0.3 ml of 0.73% w/v NaCl, vortexed, and centrifuged (10 min at $4000 \times$ g and 4°C). The aqueous phase plus debris were collected and extracted again twice with 0.8 ml chloroform, the organic phases were pooled and organic solvents were evaporated under nitrogen gas. Dried samples were reconstituted with 0.1 ml chloroform, mixed with 1 ml cold acetone, and centrifuged (10 min at $4000 \times$ g and 4°C) to precipitate proteins. The upper layer was collected and evaporated to dryness and reconstituted with 0.1 ml methanol and placed in auto-sample vials for analysis.

The Ultra performance liquid chromatography - tandem mass spectrometer (UPLC-MS/MS) analysis of AEA, 2-AG, arachidonic acid and PGD_2 was performed on a Sciex 6500 QTRAP system with an IonDrive Turbo V source for TurbolonSpray® (Ontario, Canada) attached to a Shimadzu UPLC system (Kyoto, Japan) controlled by Analyst software (Ontario, Canada). Chromatographic separation of AEA, 2-AG and arachidonic acid was performed on a Discovery® HS C18 Column 15cm x 2.1mm, 3µm (Supelco: Bellefonte, PA) kept at 25°C and a injection volume of 10 µL. The mobile phase consisted of A: acetonitrile and B: water with 1 g/L ammonium acetate and 0.1% formic acid. The following gradient was used: 0.0 to 2.4 minutes at 40% A, 2.5 to 6.0 minutes at 40% A, hold for 2.1 minutes at 40% A, then 8.1 to 9 min 100% A, hold at 100% A for 3.1 min and return to 40% A at 12.1 min with a flow rate was 1.0 mL/min. The source temperature was set at 600°C and had a curtain gas at a flow rate of 30 ml/min. The ionspray voltage was 5000 V with ion source gases 1 and 2 flow rates of 60 and 50 ml/min, respectively. The mass spectrometer was run in positive ionization mode for AEA and 2-AG and in negative ionization mode for arachidonic acid, and the acquisition mode used was multiple reaction monitoring (MRM). The following transition ions (m/z) were monitored with their corresponding collection energies (eV) in parentheses: AEA: 348>62 (13) and 348>91 (60); AEA-d_8: 356>63 (13); 2-AG: 379>287 (26) and 379>296 (28); 2-AG-d_8: 384>287 (26); arachidonic acid: 303>259 (-25) and 303>59 (-60); arachidonic acid-d_8: 311>267 (-25); PGD_2: 351>271 (-23) and 351>315 (-15); PGD_2-d_4: 355>275 (-23). The total run time for the analytical method was 14 min. Calibration curves were analyzed with each analytical batch for each analyte. A linear regression of the ratio of the peak area counts of analyte and the corresponding deuterated ISTDs versus concentration was used to construct the calibration curves.

Conditioned Place Preference

An unbiased conditioned place preference paradigm was used to examine the effects of MJN110 in control mice and in paclitaxel-treated mice (Kota *et al.*, 2007; Sanjakdar *et al.*, 2015). Following at

least one week of acclimation to the vivarium, mice were handled for three weeks leading up to CPP conditioning. A three-chamber design was utilized (two conditioning chambers with a central acclimation chamber; ENV3013, Med Associates, St Albans, VT). The outer chambers were 20 x 20 x 20 cm with differing flooring (white mesh or black rods) and wall coloring (white or black) to distinguish each. A small grey chamber in the middle connected to each outer chamber with a door.

This experiment consisted of four groups of mice in which each group received a cycle of paclitaxel or vehicle and then received conditioning sessions in which they were either administered vehicle each conditioning day or administered MJN110 or vehicle on alternating days. Eight days after the final paclitaxel injection, mice were placed in the central chamber and allowed to acclimate for 5 min. The doors to both chambers were then opened and the mouse was allowed to explore the apparatus in a drug-free state for 15 min to record baseline chamber preferences. Beginning on post paclitaxel day 9, half the mice in each group received a single daily i.p. injection of vehicle or MJN110 (5 mg/kg), alternating between these treatments each day for a total of eight conditioning sessions. MJN110 or vehicle was randomly assigned to either the black or white chamber at the start of the experiment to avoid potential bias. The other half of the mice received a single daily i.p. injection of vehicle prior to each conditioning session. One hour after each injection, each mouse was placed in the appropriate conditioning chamber for 30 min. The day after the final conditioning session, each mouse was returned to the apparatus, but did not receive an injection, and was allowed to move freely among the chambers for a 15 min test period. Preference scores were calculated for MJN110 treatment based on the total amount of time spent in the MJN110-paired side (Day 10, in s) minus the baseline preference (Day 1, in s) for the same chamber. Paclitaxel- and vehicle-treated control mice (mice received vehicle paired to both chambers), the preference score was calculated as the average of the test preferences minus the baseline preference for each chamber.

Cell culture

All lung cancer cells were maintained in DMEM supplemented with 10% (v/v) fetal bovine serum (FB22-500HI, Serum Source International, Charlotte, NC, USA) and 1% (v/v) combination of 10,000 U/ml penicillin and 10,000 μg/ml streptomycin (15140-122; Pen/Strep, ThermoFisher Scientific, Carlsbad, CA). Cells were incubated at 37°C under a humidified, 5% CO_2 atmosphere. The H460 NSCLC cell line was generously provided by the laboratory of Dr. Richard Moran at VCU and the A549 NSCLC cell line was a gift from the laboratory of Dr. Charles Chalfant at VCU.

Paclitaxel (50nM) and JZL184 (1μM) were dissolved in DMSO, diluted with sterile PBS, and added to the medium in order to obtain the desired concentrations; less than 0.1% DMSO was present in the medium. This concentration of JZL184 was chosen as it inhibits MAGL in cancer cells (Nomura *et al.*, 2010). All experiments using DMSO were performed in the dark.

Assessment of cell viability

The NSCLC cells were exposed to JZL184, paclitaxel or a combination of JZL184 and paclitaxel for 24 h, after which the drugs were removed and replaced with fresh medium. The number of viable cells was determined via trypan blue exclusion on days 1, 3, 5 and 7 post-treatment. Cells were incubated with trypsin (0.25% trypsin-EDTA) for 3 min and stained with trypan blue (15250; Invitrogen, Carlsbad, CA). The viable unstained cells were counted using a hemocytometer with bright-field microscopy.

Assessment of apoptosis

Flow cytometry analyses were performed using BD FACSCanto II (BD Biosciences, San Jose, CA) and BD FACSDiva software at the Virginia Commonwealth University Flow Cytometry Core facility. For all studies, 10,000 cells per replicate within the gated region were analyzed. When collecting samples, both adherent and floating cells were harvested with 0.1% trypsin-EDTA and neutralized with medium after 48 h of drug exposure. For quantification of apoptosis, cells were centrifuged and washed with PBS, then resuspended in 100 μl of 1x binding buffer with 5 μl of Annexin V and 5 μl of propidium iodide (556547; FITC Annexin V Apoptosis Detection Kit; BD Biosciences, San Jose, CA). The samples were then incubated at room temperature while protected from light for 15 min. The suspension solution was then brought up to 500 μl using the 1x binding buffer and analyzed by flow cytometry.

Statistical Analyses

Results are reported as the mean ± S.E.M. and were prepared using GraphPad Prism 7. ED_{50} values were calculated as previously described (Grim *et al.*, 2017). Briefly, data were converted to % Maximal Positive Effect (average maximum and minimum values for drug treatment) for each cohort and plotted versus log dose values. ED_{50} values and 95% confidence limits were calculated using a linear regression analysis. Potency ratios were calculated based on the distance between the two dose-response curves with 95% confidence limits. Based on the study design, a one- or two-way analysis of

variance (ANOVA) was used to identify statistical differences followed by Holm-Sidak *post hoc* testing of significant ANOVAs. Dunnett's test was used when comparing all treatments to a single control group in the dose-response studies. A within-subjects design was used for studies involving genetic knockouts, MJN110 time-course, KT-195 time-course and MJN110 antagonism studies. A repeated-measures ANOVA was used specifically for time-course studies and when comparing paw withdrawal thresholds pre- and post-paclitaxel. Unpaired *t* tests were used to compare two groups when indicated. Unless otherwise noted, pre-paclitaxel/vehicle baseline allodynia values were not included in statistical analysis. n=7-8 for all allodynia studies; n=15-16 per group for CPP studies; n=4 for immunohistochemistry studies. Grubbs' test was used to remove any significant outliers from each group in the CPP studies only. For all experiments, the probability of a type I error (α) was set to 5% with P values of <0.05 considered significant.

Results

MAGL inhibitors reverse paclitaxel-induced mechanical allodynia in dose- and time-dependent manners

Mice undergoing a paclitaxel cycle regimen displayed significant mechanical allodynia relative to control mice within 24 h following the final injection [main interaction of drug x F $(1, 13) = 8.71$, P<0.05 ; Supplemental Figure 1]. JZL184 (40 mg/kg, i.p.) significantly reversed paclitaxel-induced mechanical allodynia [main interaction of drug x time, F $(7, 98) = 9.50$, P<0.001] for up to five h (Figure 1A). Similarly, MJN110 (5 mg/kg, i.p.) reversed mechanical allodynia compared to vehicle treatment [main interaction of drug x time, F $(7, 98) = 6.83$, P<0.001] for up to five h post-administration (Figure 1B). In mice that did not receive paclitaxel, JZL184 (40 mg/kg) altered paw withdrawal thresholds [main interaction of drug x time, F $(7, 98) = 2.204$; P<0.05]; however, post hoc analysis did not reveal any significant differences compared to vehicle up to 24 h post-treatment (Supplemental Figure 2A). In vehicle control mice, MJN110 (5 mg/kg) did not significantly alter von Frey withdrawal thresholds [main effect of time, P=0.48; main effect of drug, P=0.61; interaction, P=0.96; Supplemental Figure 2B]. To control for ABHD6 inhibition, an off-target effect of MJN110 (Niphakis *et al.*, 2013), KT-195 (40 mg/kg) was administered to paclitaxel- and control vehicle-treated mice. KT195 did not alter paw withdrawal thresholds in either paclitaxel-treated (P>0.3) or control animals (P>0.3; Supplemental Figure 3).

The mechanical anti-allodynic dose-response relationships of JZL184 and MJN110 from separate cohorts of mice are depicted in Figure 1C. JZL184 significantly reversed paclitaxel-induced allodynia [F $(5, 42) = 5.74$, P<0.001], with 16 and 40 mg/kg.JZL184 significantly differing from the vehicle condition. JZL184 (40 mg/kg) fully reversed paclitaxel-induced allodynia and elicited similar von Frey thresholds as those from mice that did not receive paclitaxel [*t* test, P>0.05]. Similarly, MJN110 significantly reversed mechanical allodynia [F $(4, 35) = 4.83$, P<0.01],. With 3 and 5 mg/kg MJN110 statistically differing from the vehicle condition. MJN110 (5 mg/kg) fully reversed paclitaxel-induced allodynia to withdrawal thresholds comparable to control mice not treated with paclitaxel [*t* test, P>0.05]. The respective ED_{50} values (95% confidence limits) for JZL184 and MJN110 were 8.4 (5.2-13.6) and 1.8 (1.0-3.3) mg/kg,. MJN110 was 4.7 (2.0-10.6; 95% confidence limits) times more potent than JZL184.

Anti-allodynic effects of MAGL inhibitors require CB₁ receptors

A cycle of paclitaxel elicited significant mechanical allodynia in both CB_1 (+/+) and (-/-) mice [main effect of paclitaxel, $F (1, 14) = 144.2$, $P<0.001$] with no significant main effects of genotype [$P=0.06$] and no significant interaction between genotype and paclitaxel treatment ($P=0.18$; Figure 2A). Allodynia was stable during the four weeks of behavioral assessment. JZL184 significantly reversed paclitaxel-induced allodynia in CB_1 (+/+) mice, but not in CB_1 (-/-) mice [interaction of drug x genotype, $F (1, 26) = 8.316$, $P<0.01$; Figure 2A]. Similarly, MJN110 significantly reversed allodynia in CB_1 (+/+) mice, and not in CB_1 (-/-) mice [interaction of drug x genotype, $F (1, 28) = 5.574$, $P<0.05$; Figure 2A].

Using a complementary pharmacologic approach, the CB_1 receptor antagonist rimonabant (3 mg/kg) or vehicle was administered 30 min before each respective MAGL inhibitor. As shown in Figure 2B, rimonabant blocked the anti-allodynic effects of JZL184, but had no effects on its own [interaction of antagonist x drug, $F (1, 28) = 11.56$, $P<0.01$]. Similarly, rimonabant blocked the anti-allodynic effects of MJN110 [$F (1, 28) = 40.0$, $P<0.001$; Figure 2C]. However, rimonabant did not affect von Frey threshold in control mice that did not receive a cycle of paclitaxel [t test, $P>0.05$] (Figures 2B and 2C).

Anti-allodynic effects of MAGL inhibitors require CB_2 receptors

CB_2 (+/+) and (-/-) mice developed significant mechanical allodynia after a cycle of paclitaxel [main effect of paclitaxel, $F (1, 14) = 113.8$, $P<0.001$] with no difference between genotypes [$P=0.35$] (Figure 3A), and allodynic responses remained stable throughout the five week behavioral assessment period. JZL184 [interaction of drug x genotype, $F (1, 28) = 21.8$, $P<0.001$; Figure 3A] as well as MJN110 [$F (1, 28) = 9.491$, $P<0.01$; Figure 3A] significantly reversed paclitaxel-induced mechanical allodynia in CB_2 (+/+), and not in CB_2 (-/-) mice.

In the next experiment, we tested whether a CB_2 receptor antagonist would block the antinociceptive effects of these MAGL inhibitors. SR144528 (3 mg/kg, i.p.) or vehicle was administered 30 min prior to JZL184 or MJN110. As shown in Figure 3B, SR144528 blocked the anti-allodynic effects of JZL184, and lacked effects on its own [interaction of antagonist x drug, $F (1, 28) = 12.33$, $P<0.01$]. Similarly, SR144528 blocked the anti-allodynic effects of MJN110 [interaction of antagonist x drug, $F (1, 28) = 9.43$, $P<0.01$; Figure 3C]. Although SR144528 produced a significant, but small reduction in paw withdrawal thresholds in control mice in the JZL184 experiment (Figure 3B), it did not affect thresholds in control mice in the MJN110 experiment (Figure 3C).

MJN110 attenuates MCP-1 and phospho-p38 expression in paclitaxel-treated mice

As paclitaxel causes inflammatory responses in DRG (Li *et al.*, 2015; Zhang *et al.*, 2016) and spinal cord (Pevida *et al.*, 2013; Zhang *et al.*, 2013), we evaluated whether a MAGL inhibitor would attenuate this inflammation at 3 h, a time point corresponding to allodynia reversal. A cycle of paclitaxel led to a significant increase in MCP-1 expression in the DRG compared to mice that did not receive paclitaxel [interaction of paclitaxel treatment x MJN110 treatment, $F (1, 12) = 9.426$, $P<0.05$; post hoc: $P<0.01$; Figure 4A and 4B]. Treatment with MJN110 (5 mg/kg) significantly decreased MCP-1 expression in paclitaxel-treated mice [$P<0.01$], but not in the control vehicle-treated mice [$P=1.0$ for comparison between Paclitaxel-MJN110 and Control-Vehicle mice]. Paclitaxel also increased MCP-1 expression in the spinal dorsal horn, an effect that was attenuated by MJN110 pre-treatment versus vehicle [$F (1, 12) = 6.294$, $P<0.05$; post hoc $P<0.01$; Figure 5A and 5B]. MJN110 significantly decreased spinal MCP-1 expression in paclitaxel-treated mice to levels comparable to Control-Vehicle mice [$P=0.68$].

Mice given a cycle of paclitaxel also demonstrated significantly increased phospho-p38 expression in the DRG compared to control mice and this effect was inhibited by MJN110 [interaction of paclitaxel treatment x MJN110 treatment, $F (1, 12) = 16.56$, $P<0.01$; Figure 6A and 6B]. MJN110 significantly decreased DRG phospho-p38 expression in paclitaxel-treated mice to levels comparable to Control-Vehicle mice [$P=0.98$]. However, there were no significant changes in the expression of phospho-p38 MAPK in the spinal dorsal horn [no main effect of paclitaxel, $P=0.60$; no main effect of MJN110, $P=0.90$; Figure 7A and 7B]. Qualitative confocal microscopy of DRG showed that MCP-1 and phospho-p38 expression co-localizes in neurons and cells consistent with the location of satellite cells as indicated by the nuclear marker DAPI (Figure 8).

Repeated administration of low-dose JZL184 produces sustained anti-allodynic effects and increases 2-AG levels in the lumbar spinal cord

Figure 9A outlines the treatment procedure depicting the consequences of acute and repeated administration of 4 mg/kg (threshold dose) and 40 mg/kg (high dose) JZL184. These treatments produced statistically significant differential effects on paclitaxel-induced allodynia [$F (5, 42) = 8.38$, $P<0.001$; Figure 9B]. Acute administration of 40 mg/kg JZL184 fully reversed paclitaxel-induced allodynia [$P<0.01$], but this effect underwent tolerance following six days of daily administration [$P=1.0$]. In contrast, whereas acutely administered 4 mg/kg JZL184 did not significantly attenuate paclitaxel-induced allodynia [$P=1.0$], repeated administration of this dose fully reversed the allodynia [$P<0.05$].

16

Following mechanical allodynia assessment, mice were sacrificed and the L4-L6 level of the lumbar spinal cord was procured for lipid quantification. As depicted in Figure 10A, JZL184 significantly elevated 2-AG levels [$F_{(5, 42)} = 81.37$, $P<0.001$]. While acute [$P<0.001$] and repeated [$P<0.001$] administration of 40 mg/kg JZL184 elevated 2-AG levels, 4 mg/kg JZL184 significantly increased 2-AG spinal levels following repeated produced administration [$P<0.001$], but not acute administration [$P=0.09$]. Repeated administration of 40 mg/kg JZL184 led to higher 2-AG levels than acute treatment [$P<0.001$]. A significant effect was also found for spinal AEA levels [$F_{(5, 42)} = 19.25$, $P<0.001$]. Repeated administration of either 4 mg/kg [$P<0.05$] or 40 mg/kg [$P<0.001$] JZL184 (Figure 10B) produced significant increased spinal AEA levels. As shown in Figure 10C, a significant effect was found for arachidonic acid spinal levels [$F_{(5, 42)} = 6.238$, $P<0.001$]. However, repeated administration of 40 mg/kg JZL184 was the only condition that significantly different from the control condition [$P<0.01$]. Finally, a significant effect was found for PGD$_2$ [$F_{(5, 42)} = 4.591$, $P<0.01$; Figure 10D]. Post hoc analysis revealed that paclitaxel-treated mice given repeated administration of 40 mg/kg JZL184 possessed lower spinal PGD$_2$ levels in mice given repeated administration of 40 mg/kg JZL184 than vehicle control mice that did not receive paclitaxel [$P<0.001$] and mice given an acute injection of 4 mg/kg JZL184 [$P=0.03$]. Compared to vehicle control mice, paclitaxel treatment did not alter 2-AG [$P=0.98$], AEA [$P=0.95$], arachidonic acid [$P=0.81$], or PGD$_2$ [$P=0.52$] levels in the lumbar spinal cord.

MJN110 produces a conditioned place preference in paclitaxel-treated mice

In the next study, we examined whether a MAGL inhibitor produces a CPP in vehicle-treated or paclitaxel-treated mice (see Figure 11A for a schematic depicting the experimental procedure). MJN110 produced a significant place preference in paclitaxel-treated mice, but did not affect place conditioning in control mice [interaction of paclitaxel treatment x MJN110 treatment, $F_{(1, 59)} = 4.338$, $P<0.05$; Figure 11B]. As confirmed in Supplemental Figure 4, paclitaxel-treated mice had significantly lower withdrawal thresholds than vehicle-treated mice both before and after CPP training and testing [interaction of paclitaxel treatment x time, $F_{(2, 122)} = 61.54$, $P<0.001$].

JZL184 does not interfere with paclitaxel-induced growth arrest or apoptosis in non-small cell lung cancer cells

The final experiment examined whether JZL184 interferes with paclitaxel-induced growth arrest of two human NSCLC lines or has effects on its own. Consistent with its known anti-proliferative actions, paclitaxel decreased the number of viable A549 cells [interaction of treatment x day, $F_{(12, 32)}$

= 10.4, P<0.001; Figure 12A]. JZL184 did not affect viable cell number alone [P=0.94 compared to control, day 7] or in combination with paclitaxel [P=0.98 compared to paclitaxel alone; Figure 12A]. Paclitaxel also decreased the number of viable H460 cells [interaction of treatment x day, $F_{(12, 32)}$ = 115, P<0.001; Figure 12B], and JZL184 did not affect viable cell number alone [P=0.93 compared to control, day 7] or in combination with paclitaxel [P=0.93 compared to paclitaxel alone]. Likewise, JZL184 did not affect apoptotic cell population. Paclitaxel produced apoptosis in both A549 cells [main effect of paclitaxel, $F_{(1, 8)}$=194.4, P<0.001; Figure 13A] and H460 cells [main effect of paclitaxel, $F_{(1, 8)}$ = 7.549, P<0.03; Figure 13B]. JZL184 did not interfere with paclitaxel-induced apoptosis and had no effect on its own in either A549 [no main effect of JZL184 treatment, P=0.59] or H460 [no main effect of JZL184 treatment, P=0.60] cells.

Discussion

The present study replicates and extends the results of other studies showing that the MAGL inhibitor JZL184 reverses paclitaxel-induced (Slivicki *et al.*, 2017) and cisplatin-induced (Guindon *et al.*, 2013) allodynia. Here, we demonstrate that JZL184 and MJN110 fully reverse paclitaxel-induced mechanical allodynia in a manner consistent with their respective MAGL inhibitory constant estimates of 8 nM and 2.1 nM (Long *et al.*, 2009a; Niphakis *et al.*, 2013). Notably, neither MAGL inhibitor produced enhanced or depressed paw withdrawal thresholds in control mice not given paclitaxel. To control for MJN110 inhibition of ABHD6, the ABHD6 inhibitor KT195 did not affect the allodynic effects of paclitaxel. The anti-allodynic effects of each MAGL inhibitor required both CB_1 and CB_2 receptors, as demonstrated by genetic and pharmacologic approaches. MJN110 also attenuated paclitaxel-induced increases in phospho-p38 and MCP-1/CCL2 expression, suggesting a concomitant decrease of inflammatory responses with allodynia reversal. Tolerance to the anti-allodynic effects of repeated administration, noted after a high dose of JZL184, was not observed with a subthreshold dose regimen that produced anti-allodynic effects and increased spinal 2-AG and anandamide levels following repeated administration. Furthermore, MJN110 produced a CPP in paclitaxel-treated mice, but not in control animals. Lastly, we show that JZL184 treatment, at a concentration that inhibits MAGL (Nomura *et al.*, 2010), does not interfere with the antiproliferative and apoptotic effects of paclitaxel in human cell lines of NSCLC.

Here we report that the anti-allodynic effects of MJN110 and JZL184 in the paclitaxel neuropathic pain model requires activation of both CB_1 and CB_2 receptors. Likewise, both receptors are required for the antinociceptive effects of MAGL inhibitors in chronic constriction injury of the sciatic nerve (Ignatowska-Jankowska *et al.*, 2015), carrageenan (Ghosh *et al.*, 2013) and cisplatin (Guindon *et al.*, 2013) models of pain. In contrast, selective CB_2 receptor agonists fully reversed paclitaxel-induced allodynia (Rahn *et al.*, 2008; Deng *et al.*, 2015b). Similarly, pan CB_1/CB_2 receptor agonists (CP55,940; WIN55-212; Δ^9-tetrahydrocannabinol) reverse paclitaxel-induced allodynia in rodents (Pascual *et al.*, 2005; Deng *et al.*, 2015a; Deng *et al.*, 2015b). The anti-allodynic effects of CP55,940 in paclitaxel-treated mice show increased potency in CB_1 (-/-) mice compared with CB_2 (-/-) mice (Deng *et al.*, 2015), demonstrating that sufficient stimulation of either receptor alone can elicit antinociceptive effects. Thus, MAGL inhibitors may require activation of both receptors because the degree to which they elevate 2-AG may be insufficient to drive anti-allodynic responses at either receptor alone.

Paclitaxel elicits neuronal damage in DRG followed later by satellite cell hypertrophy and macrophage infiltration (Peters et al., 2007). MCP-1 promotes macrophage recruitment (Zhang et al.,

2016) and its expression in small nociceptive neurons sensitizes large- and medium-sized neurons by increasing intracellular calcium (Zhang et al., 2013). Paclitaxel also increases MCP-1 expression in the spinal dorsal horn from astrocytes (Zhang et al., 2013) as well as phosphorylates p38 through toll-like receptor 4 activation in DRG neurons, but not in the spinal cord (Li et al., 2015). Phospho-p38 expression on small IB4- and CGRP-positive neurons (Li et al., 2015) leads to sodium channel activation and hyperexcitability of nociceptive neurons (Hudmon et al., 2008). Here, we confirmed that a cycle of paclitaxel induces MCP-1 expression in both the lumbosacral DRG and lumbar dorsal horn, while phospho-p38 is increased in the DRG, but not in the dorsal horn, as previously reported (Zhang et al., 2013; Li et al., 2015). As shown in Figure 8, phospho-p38 and MCP-1 co-expression occurs in the same DRG neurons and cells consistent with the location of satellite cells. The findings that MJN110 attenuates increased expression of phospho-p38 and MCP-1 from paclitaxel indicates an anti-inflammatory action, though further work is needed to determine whether CB_1 and CB_2 receptors mediate these actions.

Whereas prolonged and complete blockade of MAGL leads to high brain levels of endocannabinoids, CB_1 receptor down-regulation and desensitization, and tolerance to the antinociceptive effects of MAGL inhibitors (Schlosburg *et al.*, 2010), repeated administration of a low dose JZL184 produces elevated endocannabinoid brain levels without CB_1 receptor functional tolerance (Kinsey *et al.*, 2013). Similarly, the present study demonstrates that anti-allodynic effects of high-dose JZL184 (40 mg/kg) in paclitaxel-treated mice undergo tolerance following repeated administration, but repeated administration a subthreshold dose of JZL184 (4 mg/kg), which given acutely did not reverse allodynia, significantly elevated 2-AG and AEA in the L4-L6 region, and fully reversed paclitaxel-induced allodynia. MAGL also contributes to the production of pro-inflammatory lipid mediators, such as arachidonic acid, prostanoids (Nomura *et al.*, 2011b), and phosphatidic acids (Nomura *et al.*, 2010), which could contribute to the anti-allodynic actions of MAGL inhibitors. However, only repeated administration of high-dose JZL814 reduced arachidonic acid in the L4-L6 region of the spinal cord, and none of the JZL184 treatments significantly affected PGD_2 compared with vehicle. Also, as paclitaxel leads to increased levels of lysophosphatidic acid (LPA) in the spinal cord dorsal horn and LPA receptor 1 (-/-) and 3 (-/-) mice show a phenotypic resistance to the development of paclitaxel-induced mechanical allodynia (Uchida *et al.*, 2014), it is possible that MAGL inhibitors reduce this lipid as well as affect other mediators.

Although thermal, chemical or mechanical stimuli are widely used to assess analgesia in rodents, these outcomes may lack clinical predictive value (Mogil, 2009). Alternatively, the CPP paradigm is

used to infer potential affective aspects of pain relief into rodent pain models (King *et al.*, 2009; Navratilova and Porreca, 2014; Havelin *et al.*, 2016). Here, we make the unique observation that the MAGL inhibitor MJN110 produces a significant place preference in paclitaxel-treated mice, but not in control mice. This pattern of findings suggests that MJN110 lacks intrinsically rewarding or aversive effects, but is rewarding in paclitaxel-treated mice. The MJN110 data from control mice are consistent with the failure of JZL184 to produce a conditioned place preference or aversion (Gamage *et al.*, 2015). The MJN110-induced CPP in paclitaxel-treated mice may represent a relief from affective or sensory aspects of nociception, as described in rodent models of cisplatin neuropathy (Park *et al.*, 2013; Krukowski *et al.*, 2017). However, MAGL inhibition may also relieve other aversive states in paclitaxel-treated mice, such as a preference for the dark chamber in the light/dark box test and increased immobility time in the forced swim test (Toma *et al.*, 2017). As MAGL inhibitors produce pharmacological effects in laboratory animal assays used to screen antidepressant and anxiolytic drugs (Kinsey *et al.*, 2011; Sciolino *et al.*, 2011; Zhong *et al.*, 2014), MJN110 chamber preference in paclitaxel-treated mice may represent relief from an aversive state distinct from neuropathy.

Because treatments for CIPN may be given while patients are still receiving chemotherapy, we tested if JZL184, at concentrations that inhibit MAGL (Nomura *et al.*, 2010), interferes with paclitaxel-induced cell death or growth arrest. We found that paclitaxel decreases cell viability and induces apoptosis in two human cell lines of NSCLC, which were not altered by JZL184. In other cancer types (i.e. prostate, melanoma, ovarian), decreased MAGL expression or activity inhibited cell proliferation and transformation (Nomura *et al.*, 2010; Nomura *et al.*, 2011a), though it is unclear whether A549 and H460 cells express MAGL. Taken together, these results suggest that inhibition of MAGL neither affects cancer growth alone nor interferes with the anti-proliferative or anti-apoptotic effects of paclitaxel in these *in vitro* models of NSCLC.

The results of the present study do not support the idea that the endogenous cannabinoid system contributes to the development of paclitaxel-induced allodynia. Consistent with previous findings (Deng *et al.*, 2015a), a cycle of paclitaxel elicited sustained mechanical allodynia in both CB_1 (-/-) and CB_2 (-/-) mice and receptor antagonists of these receptors did not alter paclitaxel-induced allodynia. The finding that a cycle of paclitaxel did not alter 2-AG and AEA spinal levels approximately two weeks later is consistent with a previous study in which paclitaxel did not alter expression of CB_1 receptor, CB_2 receptor, MAGL, or FAAH mRNA levels in spinal cord (Deng *et al.*, 2015b). In contrast, cisplatin-induced CIPN leads to increased spinal 2-AG and AEA levels (Guindon *et al.*, 2013), suggesting that the endogenous cannabinoid system differentially responds to these chemotherapeutic agents. Nonetheless,

as the present study examined only a single time point more than two weeks following paclitaxel treatment, a full time course evaluation of spinal and DRG endocannabinoid levels would be of value.

The goal of this work was to test whether MAGL inhibition reverses paclitaxel-induced allodynia as well as markers of DRG neuroinflammation. As paclitaxel neuropathies are long-lasting (Tanabe *et al.*, 2013), substantially harm quality of life, and are difficult to treat (Kim *et al*., 2015), novel analgesic strategies are needed. The present study demonstrates that MAGL inhibitors attenuate paclitaxel nociceptive-related behaviors using both mechanical allodynia and the conditioned place preference paradigm. We also show that MAGL inhibition ameliorates MCP-1 and phospho-p38 expression in the DRG. Taken together, the findings of the present study suggest that MAGL represents a viable target for possible treatment of CIPN.

Authorship Contributions

Participated in research design: Curry, Wilkerson, Bagdas, Kyte, Patel, Donvito, Gewirtz, Damaj, Lichtman

Conducted experiments: Curry, Wilkerson, Bagdas, Mustafa, Kyte, Patel, Donvito, Poklis

Contributed new reagents or analytic tools: Niphakis, Hsu, Cravatt

Performed data analysis: Curry, Wilkerson, Bagdas, Mustafa, Kyte, Patel, Poklis

Wrote or contributed to the writing of the manuscript: Curry, Wilkerson, Bagdas, Kyte, Donvito, Gewirtz, Damaj, Lichtman

References Cited

Bagdas D, Wilkerson JL, Kulkarni A, Toma W, Al Sharari S, Gul Z, Lichtman AH, Papke RL, Thakur GA, and Damaj MI (2016) The α7 nicotinic receptor dual allosteric agonist and positive allosteric modulator GAT107 reverses nociception in mouse models of inflammatory and neuropathic pain. *Br J Pharmacol* **173**:2506–2520.

Blankman JL, Simon GM, and Cravatt BF (2007) A Comprehensive Profile of Brain Enzymes that Hydrolyze the Endocannabinoid 2-Arachidonoylglycerol. *Chem Biol* **14**:1347–1356.

Bobylev I, Joshi AR, Barham M, Ritter C, Neiss WF, Hoke A, and Lehmann HC (2015) Paclitaxel inhibits mRNA transport in axons. *Neurobiol Dis* **82**:321–331.

Cravatt BF, Giang DK, Mayfield SP, Boger DL, Lerner RA, and Gilula NB (1996) Molecular characterization of an enzyme that degrades neuromodulatory fatty-acid amides. *Nature* **384**:83–87.

Crowe MS, Wilson CD, Leishman E, Prather PL, Bradshaw HB, Banks ML, and Kinsey SG (2017) The monoacylglycerol lipase inhibitor KML29 with gabapentin synergistically produces analgesia in mice. *Br J Pharmacol*, doi: 10.1111/bph.14055.

Deng L, Cornett BL, Mackie K, and Hohmann AG (2015) CB 1 Knockout Mice Unveil Sustained CB 2 -Mediated Antiallodynic Effects of the Mixed CB 1 / CB 2 Agonist CP55, 940 in a Mouse Model of Paclitaxel-Induced Neuropathic Pain. *Mol Pharmacol* **88**:64–74.

Deng L, Guindon J, Cornett BL, Makriyannis A, Mackie K, and Hohmann AG (2015) Chronic Cannabinoid Receptor 2 Activation Reverses Paclitaxel Neuropathy Without Tolerance or Cannabinoid Receptor 1-Dependent Withdrawal. *Biol Psychiatry* **77**:475–487.

Dinh TP, Carpenter D, Leslie FM, Freund TF, Katona I, Sensi SL, Kathuria S, and Piomelli D (2002) Brain monoglyceride lipase participating in endocannabinoid inactivation. *Proc Natl Acad Sci* **99**:10819–10824.

Dougherty PM, Cata JP, Cordella JV, Burton A, and Weng HR (2004) Taxol-induced sensory disturbance is characterized by preferential impairment of myelinated fiber function in cancer patients. *Pain* **109**:132–142.

Ettinger DS and Akerley W (2010) Small cell lung cancer clinical practice guidelines in oncology. *J Natl Compr Canc Netw* **8**:602–22.

Gamage TF, Ignatowska-Jankowska BM, Muldoon PP, Cravatt BF, Damaj MI, and Lichtman AH (2015) Differential effects of endocannabinoid catabolic inhibitors on morphine withdrawal in mice. *Drug Alcohol Depend* **146**:7–16.

Ghersi D, Willson Melina L, Chan Matthew Ming K, Simes J, Donoghue E, and Wilcken N (2015) Taxane-containing regimens for metastatic breast cancer. *Cochrane Database Syst Rev*. doi: 10.1002/14651858.CD003366.pub3.

Ghosh S, Wise LE, Chen Y, Gujjar R, Mahadevan A, Cravatt BF, and Lichtman AH (2013) The monoacylglycerol lipase inhibitor JZL184 suppresses inflammatory pain in the mouse carrageenan model. *Life Sci* **92**:498–505.

Grim TW, Morales AJ, Thomas BF, Wiley JL, Endres GW, Negus SS, and Lichtman AH (2017) Apparent CB1 receptor rimonabant affinity estimates: combination with THC and synthetic cannabinoids in the mouse in vivo triad model. *J Pharmacol Exp Ther* **363**:210–218.

Guindon J, Lai Y, Takacs SM, Bradshaw HB, and Hohmann AG (2013) Alterations in endocannabinoid tone following chemotherapy-induced peripheral neuropathy: Effects of endocannabinoid deactivation inhibitors targeting fatty-acid amide hydrolase and monoacylglycerol lipase in comparison to reference analgesics following cisplatin treatment. *Pharmacol Res* **67**:94–109.

Havelin J, Imbert I, Cormier J, Allen J, Porreca F, and King T (2016) Central sensitization and neuropathic features of ongoing pain in a rat model of advanced osteoarthritis. *J Pain* **17**:374–382.

Hsu K-L, Tsuboi K, Adibekian A, Pugh H, Masuda K, and Cravatt BF (2012) DAGLβ inhibition perturbs a lipid network involved in macrophage inflammatory responses. *Nat Chem Biol* **8**:999–

1007.

Hudmon A, Choi JS, Tyrrell L, Black JA, Rush AM, Waxman SG, and Dib-Hajj SD (2008) Phosphorylation of sodium channel Na(v)1.8 by p38 mitogen-activated protein kinase increases current density in dorsal root ganglion neurons. *J Neurosci* **28**:3190–3201.

Huisman C, Ferreira CG, Bröker LE, Bro LE, Rodriguez JA, Smit EF, Postmus PE, Kruyt FA, and Giaccone G (2002) Paclitaxel Triggers Cell Death Primarily via Caspase-independent Routes in the Non-Small Cell Lung Cancer Cell Line NCI-H460 Paclitaxel Triggers Cell Death Primarily via Caspase-independent Routes in the Non-Small Cell Lung Cancer Cell Line NCI-H460 1. *Clin Cancer Res* **8**:596–606.

Ignatowska-Jankowska B, Wilkerson JL, Mustafa M, Abdullah R, Niphakis M, Wiley JL, Cravatt BF, and Lichtman AH (2015) Selective Monoacylglycerol Lipase Inhibitors: Antinociceptive versus Cannabimimetic Effects in Mice. *J Pharmacol Exp Ther* **353**:424–432.

Jung H, Toth PT, White FA, and Miller RJ (2008) Monocyte chemoattractant protein-1 functions as a neuromodulator in dorsal root ganglia neurons. *J Neurochem* **104**:254–263.

Kim JH, Dougherty PM, and Abdi S (2015) Basic science and clinical management of painful and non-painful chemotherapy-related neuropathy. *Gynecol Oncol* **136**:453-459.

King T, Vera-Portocarrero L, Gutierrez T, Vanderah TW, Dussor G, Lai J, Fields HL, and Porreca F (2009) Unmasking the tonic-aversive state in neuropathic pain. *Nat Neurosci* **12**:1364–1366.

Kinsey SG, O'Neal ST, Long JZ, Cravatt BF, and Lichtman AH (2011) Inhibition of endocannabinoid catabolic enzymes elicits anxiolytic-like effects in the marble burying assay. *Pharmacol Biochem Behav* **98**:21–27.

Kinsey SG, Wise LE, Ramesh D, Abdullah RA, Selley DE, Cravatt BF, and Lichtman AH (2013) Repeated low-dose administration of the monoacylglycerol lipase inhibitor JZL184 retains cannabinoid receptor type 1-mediated antinociceptive and gastroprotective effects. *J Pharmacol Exp Ther* **345**:492–501.

Kota D, Martin BR, Robinson SE, and Damaj MI (2007) Nicotine Dependence and Reward Differ between Adolescent and Adult Male Mice. *J Pharmacol Exp Ther* **322**:399–407.

Krukowski K, Ma J, Golonzhka O, Laumet GO, Gutti T, van Duzer JH, Mazitschek R, Jarpe MB, Heijnen CJ, and Kavelaars A (2017) HDAC6 inhibition effectively reverses chemotherapy-induced peripheral neuropathy. *Pain* **158**:1126–1137.

Li Y, Zhang H, Kosturakis AK, Cassidy RM, Zhang H, Kennamer-Chapman RM, Jawad AB, Colomand CM, Harrison DS, and Dougherty PM (2015) MAPK signaling downstream to TLR4 contributes to paclitaxel-induced peripheral neuropathy. *Brain Behav Immun* **49**:255–266.

Li Y, Zhang H, Zhang H, Kosturakis AK, Jawad AB, and Dougherty PM (2014) Toll-like receptor 4 signaling contributes to Paclitaxel-induced peripheral neuropathy. *J Pain* **15**:712–725.

Long JZ, Li W, Booker L, Burston JJ, Kinsey SG, Schlosburg JE, Pavón FJ, Serrano AM, Selley DE, Parsons LH, Lichtman AH, and Cravatt BF (2009) Selective blockade of 2-arachidonoylglycerol hydrolysis produces cannabinoid behavioral effects. *Nat Chem Biol* **5**:37–44.

Long JZ, Nomura DK, and Cravatt BF (2009) Characterization of Monoacylglycerol Lipase Inhibition Reveals Differences in Central and Peripheral Endocannabinoid Metabolism. *Chem Biol* **16**:744–753.

Makker PG, Duffy SS, Lees JG, Perera CJ, Tonkin RS, Butovsky O, Park SB, Goldstein D, and Moalem-Taylor G (2017) Characterisation of immune and neuroinflammatory changes associated with chemotherapy-induced peripheral neuropathy. *PLoS One* **12**:1–24.

Marostica LL, Silva IT, Kratz JM, Persich L, Geller FC, Lang KL, Caro MSB, Durán FJ, Schenkel EP, and Simões CMO (2015) Synergistic Antiproliferative Effects of a New Cucurbitacin B Derivative and Chemotherapy Drugs on Lung Cancer Cell Line A549. *Chem Res Toxicol* **28**:1949–1960.

Mechoulam R, Ben-Shabat S, Hanus L, Ligumsky M, Kaminski NE, Schatz AR, Gopher A, Almog S,

Martin BR, Compton DR, Pertwee RG, Griffin G, Bayewitch M, Barg J, and Vogel Z (1995) Identification of an endogenous 2-monoglyceride, present in canine gut, that binds to cannabinoid receptors. *Biochem Pharmacol* **50**:83–90.

Mogil JS (2009) Animal models of pain: progress and challenges. *Nat Rev Neurosci* **10**:283–294.

Navratilova E, and Porreca F (2014) Reward and motivation in pain and pain relief. *Nat Publ Gr* **17**:1304–1312.

Niphakis MJ, Cognetta AB, Chang JW, Buczynski MW, Parsons LH, Byrne F, Burston JJ, Chapman V, and Cravatt BF (2013) Evaluation of NHS carbamates as a potent and selective class of endocannabinoid hydrolase inhibitors. *ACS Chem Neurosci* **4**:1322–1332.

Nomura DK, Lombardi DP, Chang JW, Niessen S, Ward AM, Long JZ, Hoover HH, and Cravatt BF (2011) Monoacylglycerol lipase exerts dual control over endocannabinoid and fatty acid pathways to support prostate cancer. *Chem Biol* **18**:846–856.

Nomura DK, Long JZ, Niessen S, Hoover HS, Ng SW, and Cravatt BF (2010) Monoacylglycerol Lipase Regulates a Fatty Acid Network that Promotes Cancer Pathogenesis. *Cell* **140**:49–61.

Nomura DK, Morrison BE, Blankman JL, Long JZ, Kinsey SG, Lichtman AH, Conti B, and Cravatt BF (2011) Endocannabinoid Hydrolysis Generates Brain Prostaglandins That Promote Neuroinflammation. *Science* **334**:809–814.

Park CH, Shin TK, Lee HY, Kim SJ, and Lee WS (2011) Matrix metalloproteinase inhibitors attenuate neuroinflammation following focal cerebral ischemia in mice. *Korean J Physiol Pharmacol* **15**:115–122.

Park HJ, Stokes JA, Pirie E, Skahen J, Shtaerman Y, and Yaksh TL (2013) Persistent hyperalgesia in the cisplatin-treated mouse as defined by threshold measures, the conditioned place preference paradigm, and changes in dorsal root ganglia activated transcription factor 3: The effects of gabapentin, ketorolac, and etanercept. *Anesth Analg* **116**:224–231.

Pascual D, Goicoechea C, Suardíaz M, and Martín MI (2005) A cannabinoid agonist, WIN 55,212-2, reduces neuropathic nociception induced by paclitaxel in rats. *Pain* **118**:23–34.

Peters CM, Jimenez-Andrade JM, Kuskowski MA, Ghilardi JR, and Mantyh PW (2007) An evolving cellular pathology occurs in dorsal root ganglia, peripheral nerve and spinal cord following intravenous administration of paclitaxel in the rat. *Brain Res* **1168**:46–59.

Pevida M, Lastra A, Hidalgo A, Baamonde A, and Menéndez L (2013) Spinal CCL2 and microglial activation are involved in paclitaxel-evoked cold hyperalgesia. *Brain Res Bull* **95**:21–27.

Rahn EJ, Zvonok AM, Thakur G a, Khanolkar AD, Makriyannis A, and Hohmann AG (2008) Selective activation of cannabinoid CB2 receptors suppresses neuropathic nociception induced by treatment with the chemotherapeutic agent paclitaxel in rats. *J Pharmacol Exp Ther* **327**:584–591.

Ramesh D, Ross GR, Schlosburg JE, Owens RA, Abdullah RA, Kinsey SG, Long JZ, Nomura DK, Sim-Selley LJ, Cravatt BF, Akbarali HI, and Lichtman AH (2011) Blockade of endocannabinoid hydrolytic enzymes attenuates precipitated opioid withdrawal symptoms in mice. *J Pharmacol Exp Ther* **339**:173–85.

Samudio-Ruiz SL, Allan AM, Valenzuela CF, Perrone-Bizzozero NI, and Caldwell KK (2009) Prenatal ethanol exposure persistently impairs NMDA receptor-dependent activation of extracellular signal-regulated kinase in the mouse dentate gyrus. *J Neurochem* **109**:1311–1323.

Sanjakdar SS, Maldoon PP, Marks MJ, Brunzell DH, Maskos U, McIntosh JM, Bowers MS, and Damaj MI (2015) Differential Roles of α6β2* and α4β2* Neuronal Nicotinic Receptors in Nicotine- and Cocaine-Conditioned Reward in Mice. *Neuropsychopharmacology* **40**:350–360.

Schlosburg JE, Blankman JL, Long JZ, Nomura DK, Pan B, Kinsey SG, Nguyen PT, Ramesh D, Booker L, Burston JJ, Thomas EA, Selley DE, Sim-Selley LJ, Liu Q, Lichtman AH, and Cravatt BF (2010) Chronic monoacylglycerol lipase blockade causes functional antagonism of the endocannabinoid system. *Nat Neurosci* **13**:1113–1119.

Sciolino NR, Zhou W, and Hohmann AG (2011) Enhancement of endocannabinoid signaling with JZL184, an inhibitor of the 2-arachidonoylglycerol hydrolyzing enzyme monoacylglycerol lipase, produces anxiolytic effects under conditions of high environmental aversiveness in rats. *Pharmacol Res* **64**:226–234.

Seretny M, Currie GL, Sena ES, Ramnarine S, Grant R, MacLeod MR, Colvin LA, and Fallon M (2014) Incidence, prevalence, and predictors of chemotherapy-induced peripheral neuropathy: A systematic review and meta-analysis. *Pain* **155**:2461–2470.

Shi C, Liu Y, Zhang W, Lei Y, Lu C, Sun R, Sun Y, Jiang M, Gu X, and Ma Z (2017) Intraoperative electroacupuncture relieves remifentanil-induced postoperative hyperalgesia via inhibiting spinal glial activation in rats. *Mol Pain* **13**:1–11.

Slivicki RA, Xu Z, Kulkarni PM, Pertwee RG, Mackie K, Thakur GA, and Hohmann AG (2017) Positive Allosteric Modulation of Cannabinoid Receptor Type 1 Suppresses Pathological Pain Without Producing Tolerance or Dependence. *Biol Psychiatry* **11**:1–12.

Sugiura T, Kondo S, Sukagawa A, Nakane S, Shinoda A, Itoh K, Yamashita A, and Waku K (1995) 2-Arachidonoylglycerol: a possible endogenous cannabinoid receptor ligand in brain. *Biochem Biophys Res Commun* **215**:89–97.

Tanabe Y, Hashimoto K, Shimizu C, Hirakawa A, Harano K, Yunokawa M, Yonemori K, Katsumata N, Tamura K, Ando M, Kinoshita T, and Fujiwara Y (2013) Paclitaxel-induced peripheral neuropathy in patients receiving adjuvant chemotherapy for breast cancer. *Int J Clin Oncol* **18**:132–138.

Toma W, Kyte SL, Bagdas D, Alkhlaif Y, Alsharari SD, Lichtman AH, Chen ZJ, Del Fabbro E, Bigbee JW, Gewirtz DA, and Damaj MI (2017) Effects of paclitaxel on the development of neuropathy and affective behaviors in the mouse. *Neuropharmacology* **117**:305–315.

Uchida H, Nagai J, and Ueda H (2014) Lysophosphatidic acid and its receptors LPA1 and LPA3 mediate paclitaxel-induced neuropathic pain in mice. *Mol Pain* **10**:71.

Wilkerson JL, Gentry KR, Dengler EC, Wallace JA, Kerwin AA, Kuhn MN, Zvonok AM, Thakur GA, Makriyannis A, and Milligan ED (2012) Immunofluorescent spectral analysis reveals the intrathecal cannabinoid agonist, AM1241, produces spinal anti-inflammatory cytokine responses in neuropathic rats exhibiting relief from allodynia. *Brain Behav* **2**:155–177.

Wilkerson JL, Ghosh S, Bagdas D, Mason BL, Crowe MS, Hsu KL, Wise LE, Kinsey SG, Damaj MI, Cravatt BF, and Lichtman AH (2016) Diacylglycerol lipase beta inhibition reverses nociceptive behaviour in mouse models of inflammatory and neuropathic pain. *Br J Pharmacol* **173**:1678–1692.

Wilkerson JL, Niphakis MJ, Grim TW, Mustafa MA, Abdullah RA, Poklis JL, Dewey WL, Akbarali HI, Banks ML, Wise LE, Cravatt BF, and Lichtman AH (2016) The selective monoacylglycerol lipase inhibitor MJN110 produces opioid sparing effects in a mouse neuropathic pain model. *J Pharmacol Exp Ther* **357**:145–156.

Zhang H, Boyette-Davis JA, Kosturakis AK, Li Y, Yoon SY, Walters ET, and Dougherty PM (2013) Induction of monocyte chemoattractant protein-1 (mcp-1) and its receptor ccr2 in primary sensory neurons contributes to paclitaxel-induced peripheral neuropathy. *J Pain* **14**:1031–1044.

Zhang H, Li Y, de Carvalho-Barbosa M, Kavelaars A, Heijnen CJ, Albrecht PJ, and Dougherty PM (2016) Dorsal root ganglion infiltration by macrophages contributes to paclitaxel chemotherapy induced peripheral neuropathy. *J Pain* **17**:775–786.

Zhang H, Yoon SY, Zhang H, and Dougherty PM (2012) Evidence that spinal astrocytes but not microglia contribute to the pathogenesis of paclitaxel-induced painful neuropathy. *J Pain* **13**:293–303.

Zhong P, Wang W, Pan B, Liu X, Zhang Z, Long JZ, Zhang H-T, Cravatt BF, and Liu Q-S (2014) Monoacylglycerol Lipase Inhibition Blocks Chronic Stress-Induced Depressive-Like Behaviors via Activation of mTOR Signaling. *Neuropsychopharmacology* **39**:1763–1776.

Zimmer AM, Hohmann AG, Herkenham M, and Bonner TI (1999) Increased mortality, hypoactivity, and hypoalgesia in cannabinoid CB1 receptor knockout mice. *Proc Natl Acad Sci U S A* **96**:5780–5785.

Zoja C, Liu X-H, Donadelli R, Abbate M, Testa D, Corna D, Taraboletti G, Vecchi A, Dong QG, Rollins BJ, Bernati T, and Remuzzi G (1997) Renal Expression of Monocyte Chemoattractant Protein-1 in Lupus Autoummune Mice. *J Am Soc Nephrol* **8**:720–729.

Footnotes

Figure Legends

Figure 1. MAGL inhibitors significantly reverse mechanical allodynia in paclitaxel-treated mice. (**A**) JZL184 (40 mg/kg) reverses paclitaxel-induced allodynia with maximal anti-allodynic effects occurring from 0.5 to 5 h post administration compared to baseline (BL). (**B**) MJN110 reverses mechanical allodynia with maximal effects occurring 2 to 5 h post injection. Pre-Pac= baseline prior to paclitaxel (Pac) treatment. (**C**) JZL184 and MJN110 dose-dependently reverse mechanical allodynia in separate cohorts of paclitaxel-treated mice. Maximum reversal of allodynia was comparable to vehicle control mice treated with vehicle (Ctrl-Veh) for both drugs, as they did not significantly differ. Data are reported as mean ± S.E.M., n = 7-8 mice/group. *P<0.05, **P<0.01, ***P<0.001 versus vehicle-treated mice at the respective time point (**A** and **B**). Filled symbols indicate a significant effect (P<0.05) of drug versus vehicle-treated mice that received a cycle of paclitaxel (**C**).

Figure 2. The anti-allodynic effects of MAGL inhibitors require CB_1 receptor activation. (**A**) A cycle of paclitaxel (Pac) leads to the development of mechanical allodynia in CB_1 (+/+) and (-/-) mice. JZL184 and MJN110 significantly reverse mechanical allodynia in CB_1 (+/+) mice, but not in CB_1 (-/-) mice. The CB_1 receptor antagonist rimonabant significantly blocks the anti-allodynic effects of JZL184 (**B**) and MJN110 (**C**). Control (Ctrl) mice and vehicle (Veh) treatment groups are shown for comparison. Data are reported as mean ± S.E.M., *n* = 7-8 mice/group. *P<0.05 versus CB_1 (+/+) mice (**A**). ***P<0.001 versus vehicle pre-treatment (**B** and **C**).

Figure 3. The anti-allodynic effects of MAGL inhibitors require CB_2 receptor activation. (**A**) A cycle of paclitaxel (Pac) leads to the development of mechanical allodynia in CB_2 (+/+) and (-/-) mice. JZL184 and MJN110 lack anti-allodynic effects in CB_2 (-/-) mice, but fully reverse paclitaxel-induced mechanical allodynia in CB_2 (+/+) animals. The CB_2 receptor antagonist SR144528 blocks the anti-allodynic effects of JZL184 and MJN110. Control (Ctrl) mice and vehicle (Veh) treatment groups are shown for comparison. Data are reported as mean ± S.E.M., *n* = 8 mice/group. ***P<0.001 versus CB_2 (+/+) mice (**A**). *P<0.05, ***P<0.001 versus vehicle pre-treatment (**B** and **C**).

Figure 4. MJN110 attenuates paclitaxel-induced MCP-1 expression in the dorsal root ganglia. (**A**) Nine days after a cycle of paclitaxel, vehicle-treated mice show a significant increase of MCP-1 expression in lumbosacral dorsal root ganglia compared to control mice that did not receive paclitaxel. MJN110

30

significantly blocks paclitaxel-induced increases of MCP-1 expression. (**B**) Representative dorsal root ganglia image for each of the four treatment conditions. All images are at 40x. Scale bar = 10μm. Data are reported as mean ± S.E.M., *n* = 4 mice/group. **P<0.01 versus vehicle-treated mice that did not receive paclitaxel. ##P<0.01 versus vehicle-treated mice that received paclitaxel.

Figure 5. MJN110 attenuates paclitaxel-induced MCP-1 expression in the dorsal horn of the spinal cord. (**A**) A cycle of paclitaxel elicits a significant increase in MCP-1 expression in lumbosacral spinal cord compared to control mice that did not receive paclitaxel. MJN110 (5 mg/kg) reverses paclitaxel-induced elevations of MCP-1 expression. (**B**) Representative image for each of the four conditions. All images are at 40x. Scale bar = 10 μm. Data are reported as mean ± S.E.M., *n* = 4 mice/group. **P<0.01 versus vehicle-treated mice that did not receive paclitaxel. ##P<0.01 versus vehicle-treated mice that received paclitaxel.

Figure 6. MJN110 attenuates paclitaxel-induced phospho-p38 MAPK expression in the dorsal root ganglia. (**A**) Following paclitaxel treatment, vehicle-treated mice show a significant increase of phospho-p38 expression in lumbosacral dorsal root ganglia compared to control mice that did not receive paclitaxel. MJN110 significantly decreased paclitaxel-induced expression of phospho-p38. (**B**) Representative dorsal root ganglia image for each of the four conditions. All images are at 40x. Scale bar = 10 μm. Data are reported as mean ± S.E.M., *n* = 4 mice/group. ***P<0.001 versus vehicle-treated mice that did not receive paclitaxel. ###P<0.001 versus vehicle-treated mice that received paclitaxel.

Figure 7. Paclitaxel does not increase phospho-p38 expression in the spinal dorsal horn. (**A**) Neither paclitaxel nor MJN110 alters phosphorylated phospho-38 MAPK expression in the spinal dorsal horn. (**B**) Representative images for each condition. All images are at 40x. Scale bar = 10μm. Data are reported as mean ± S.E.M., n = 4 mice/group.

Figure 8. Qualitative confocal microscopy of MCP-1 and phospho-p38 MAPK co-localization in dorsal root ganglia cells. A cycle of paclitaxel (Pac) increased MCP-1 (left) and phospho-p38 (middle) expression compared to control vehicle (Ctrl) treatment. MCP-1 and phospho-p38 co-localize in cells stained with the nuclear marker DAPI (right). Thick arrows indicate neurons, and thin arrows indicate cells consistent with the location of satellite cells. This co-localization is not observed in sections from

MJN110 (MJN)-treated mice compared to vehicle (Veh) treatment. All images are at 63x. Scale bar = 10μm.

Figure 9. Acute and repeated administration of 4 and 40 mg/kg JZL184 differentially affect paclitaxel-induced allodynia. (**A**) Experimental procedural timeline. (**B**) Although acute administration of high-dose JZL184 fully reverses paclitaxel-induced allodynia, this antinociceptive effect undergoes tolerance following six days of daily JZL184. Whereas acute administration of low-dose JZL184 does not attenuate paclitaxel-induced allodynia, it completely reverses allodynia after repeated administration. All data were recorded two hours after the last treatment. Data are reported as mean ± S.E.M., $n = 8$ mice/group. *P<0.05, **P<0.01 versus the corresponding acute condition; ##P<0.01 versus no paclitaxel.

Figure 10. Acute versus repeated administration of JZL184 (4 or 40 mg/kg) on (**A**) 2-AG, (**B**) anandamide (AEA), (**C**) arachidonic acid, and (**D**) prostaglandin D2 (PGD$_2$) in spinal cord. Data are reported as mean ± S.E.M., $n = 8$ mice/group. *P<0.05, **P<0.01***P<0.001 versus Paclitaxel-Vehicle. #P<0.05, ###P<0.001 versus the corresponding acute treatment.

Figure 11. A MAGL inhibitor produces a conditioned place preference in paclitaxel-treated mice. (**A**) Conditioned place preference procedure. (**B**) MJN110 (5 mg/kg) leads to the development of a CPP in paclitaxel-treated mice, but not in mice that received a cycle of vehicle a CPP in paclitaxel-treated. BL = baseline preference test prior to conditioning. Test = drug-free preference test after conditioning. Data are reported as mean ± S.E.M., $n = 15-16$ mice/group. *P<0.05 MJN110 vs vehicle control in paclitaxel mice.

Figure 12. JZL184 does not stimulate non-small cell lung cancer (NSCLC) cell proliferation alone or interfere with paclitaxel (Pac, 50nM)-induced growth inhibition of (**A**) A549 or (**B**) H460 cells. Day 0 represents the initial number of cells after seeding. JZL184 (1 μM), paclitaxel or the combination of paclitaxel and JZL184 was added to the cultures on day 0 and was replaced with drug-free medium 24 hours later. The number of viable cells was determined via trypan blue exclusion. Data are expressed as the mean ± SEM of three independent experiments. ***P<0.001 versus control.

Figure 13. JZL184 does not affect paclitaxel-induced apoptosis of non-small cell lung cancer (NSCLC) cells. (**A**) fp30p30A549 and (**B**) H460 cells were exposed to JZL184 (1 μM), paclitaxel (100 nM), or the combination of paclitaxel and JZL184 for 48 h. Quantification of apoptotic cells was determined using the Annexin V/PI assay, followed by flow cytometry analysis. Data are expressed as mean ± SEM of three independent experiments.
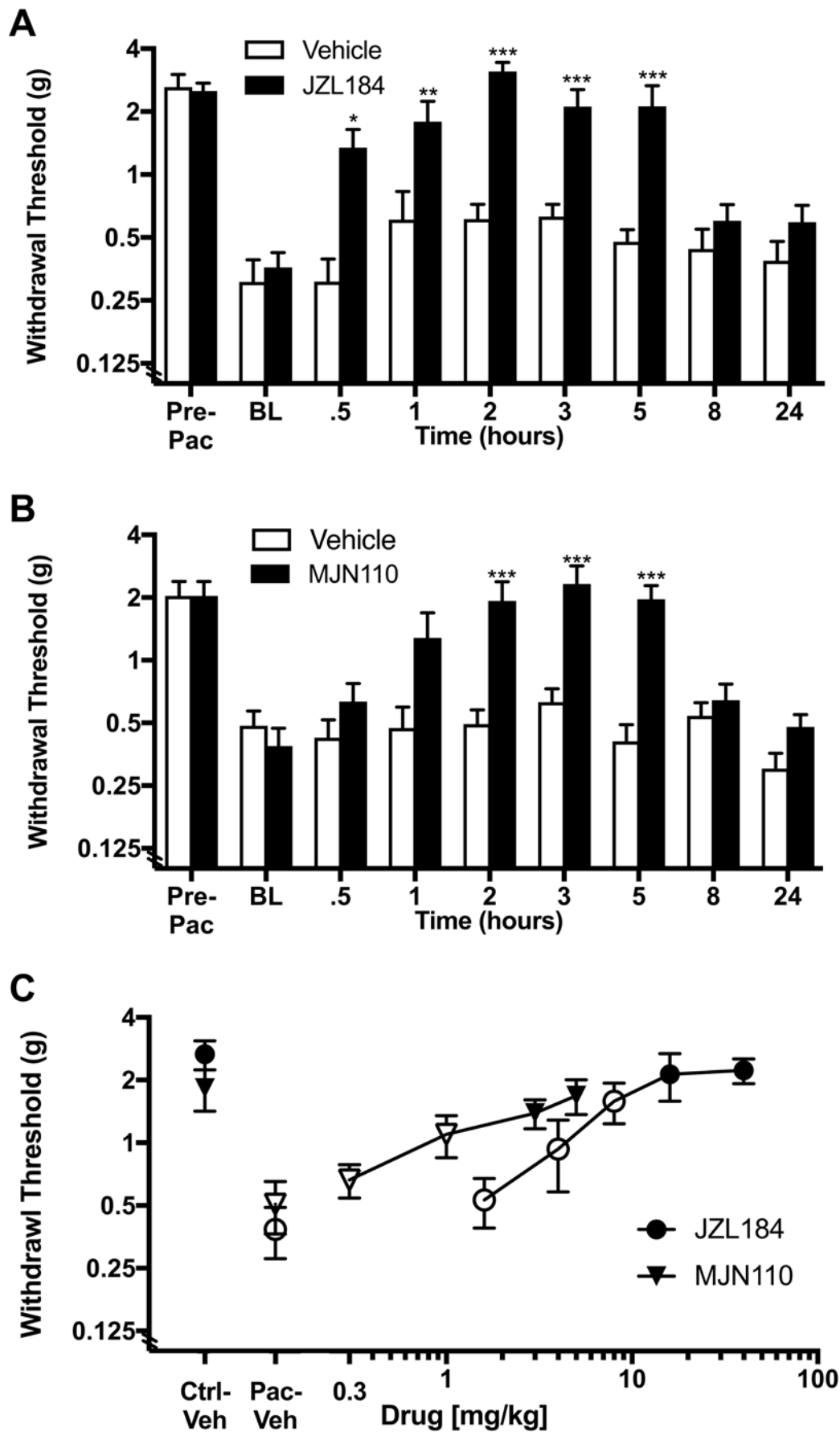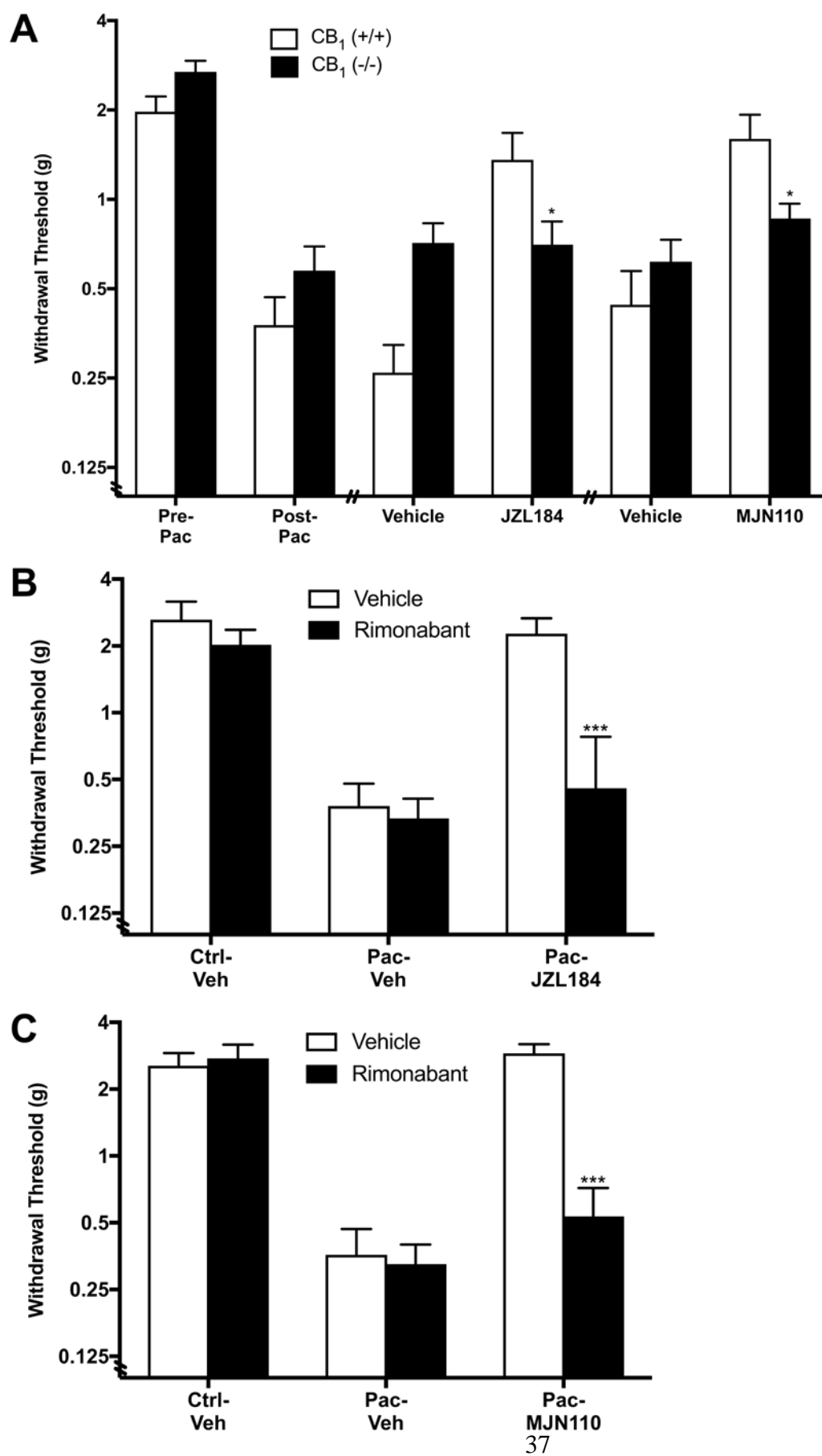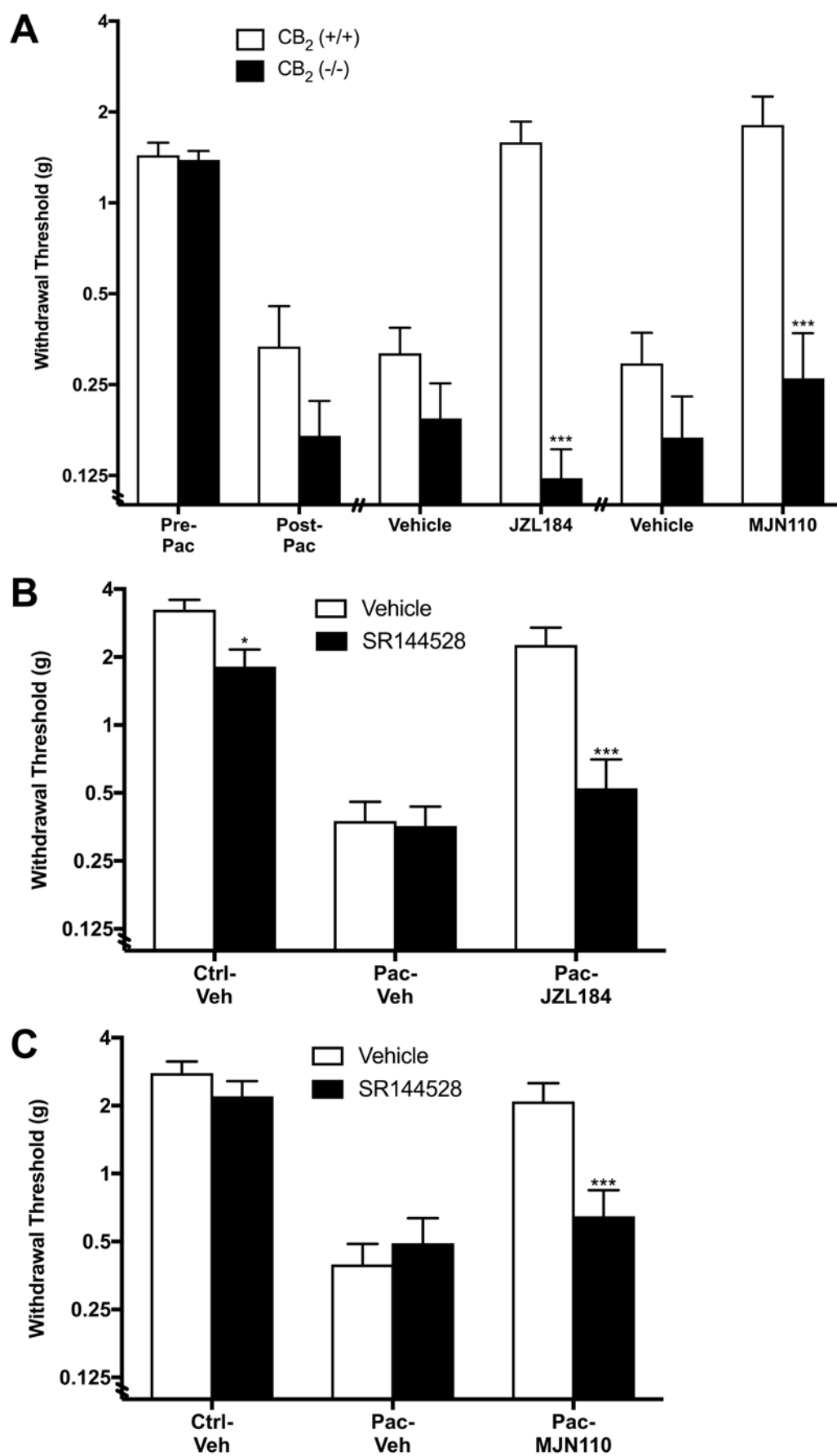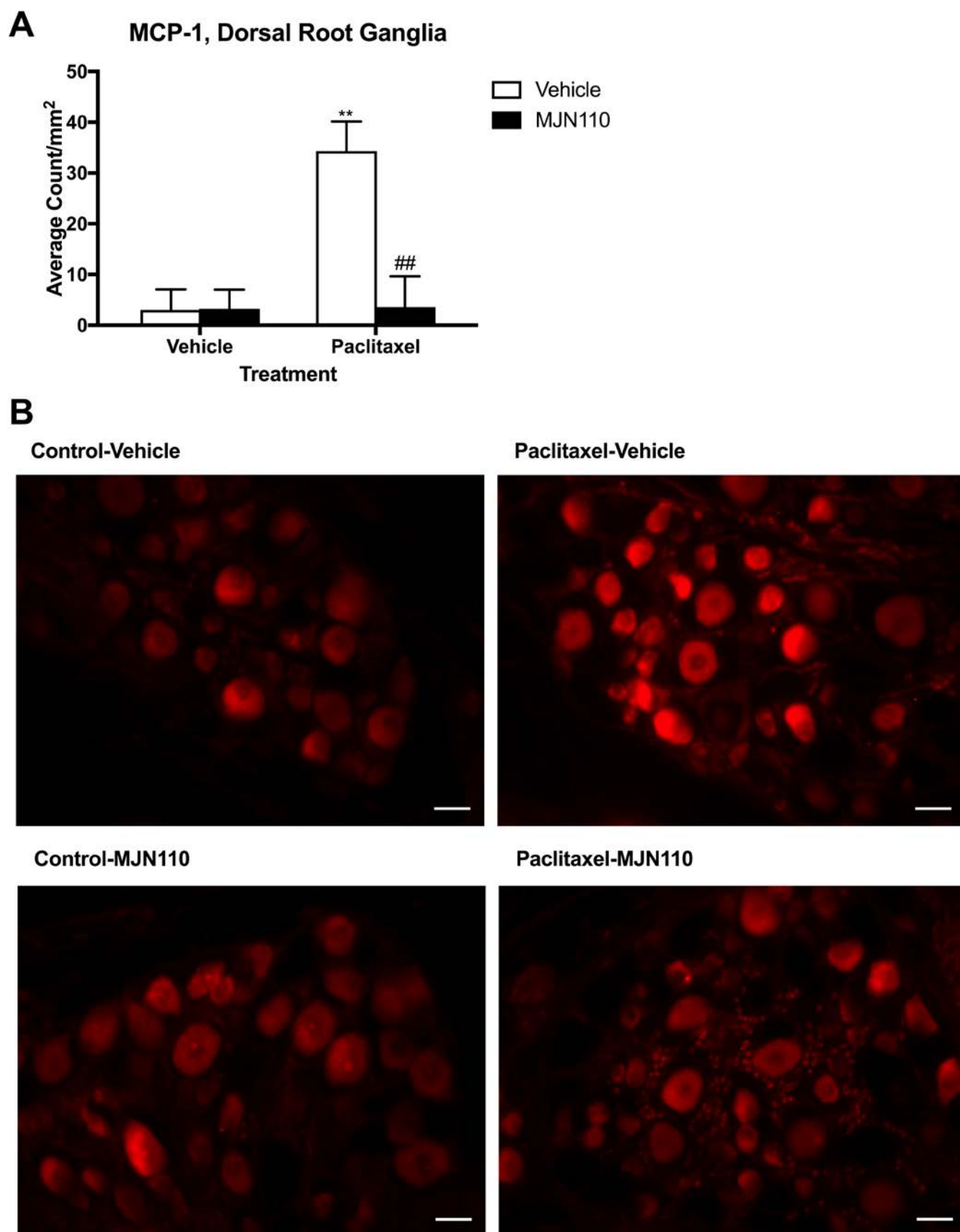
Figure 1

Figure 2

Figure 3

Figure 4

A MCP-1, Dorsal Root Ganglia

B

Control-Vehicle   Paclitaxel-Vehicle

Control-MJN110   Paclitaxel-MJN110

Figure 5

Figure 6

Figure 7

A

phospho-p38 MAPK, Dorsal Horn

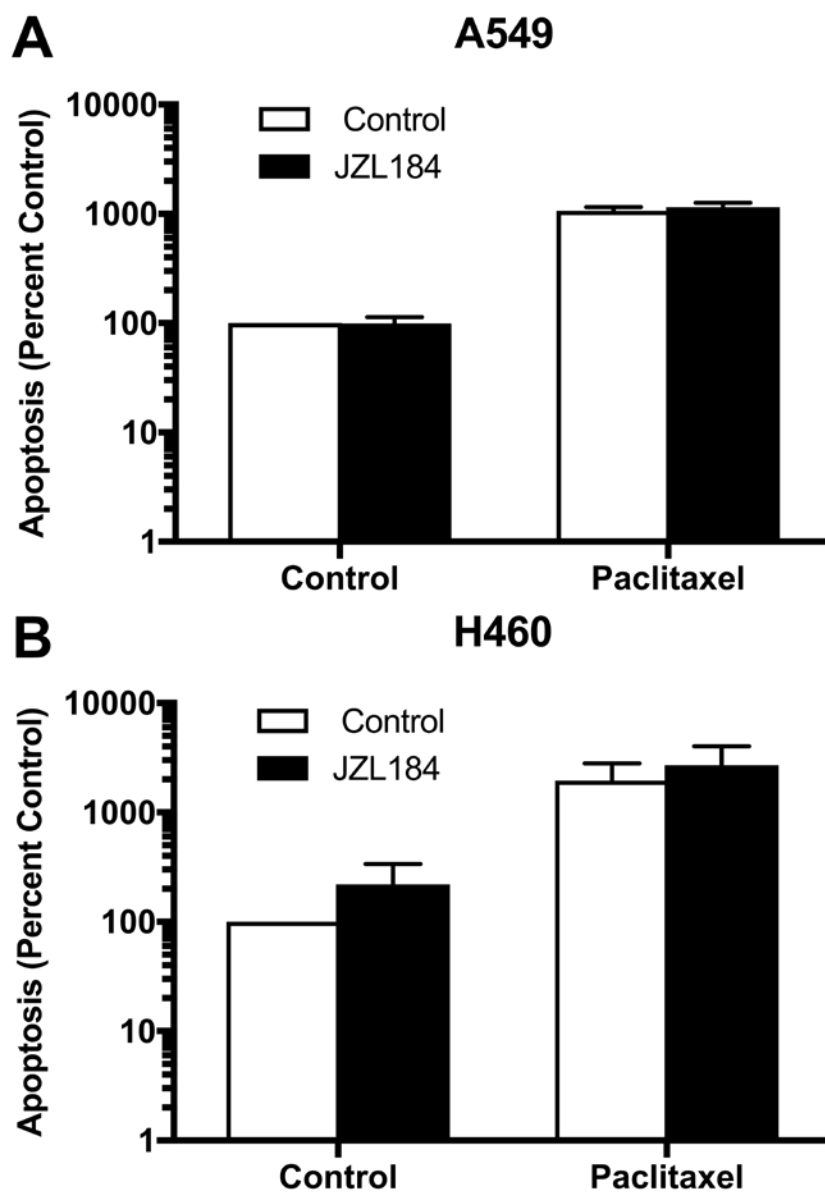**B**
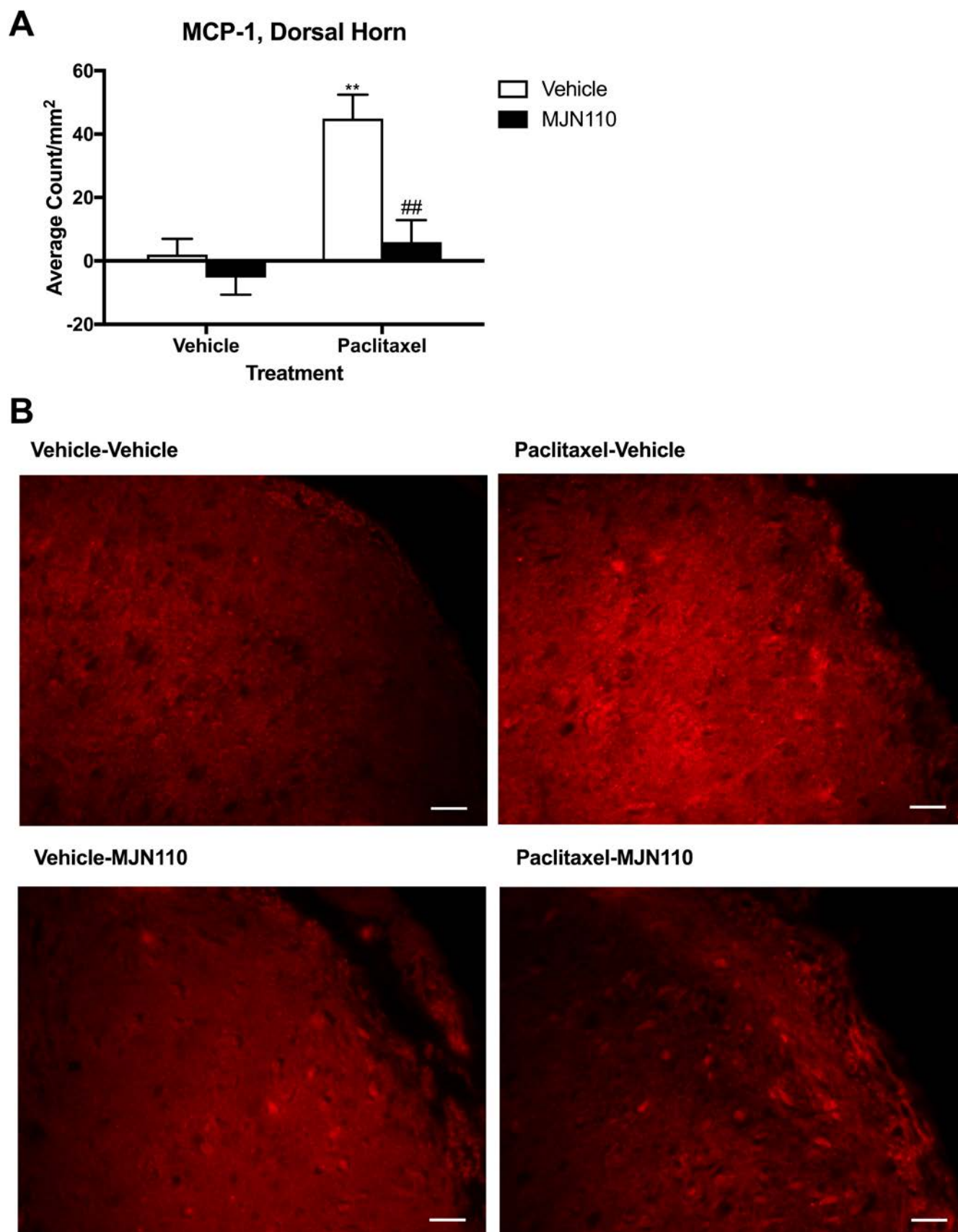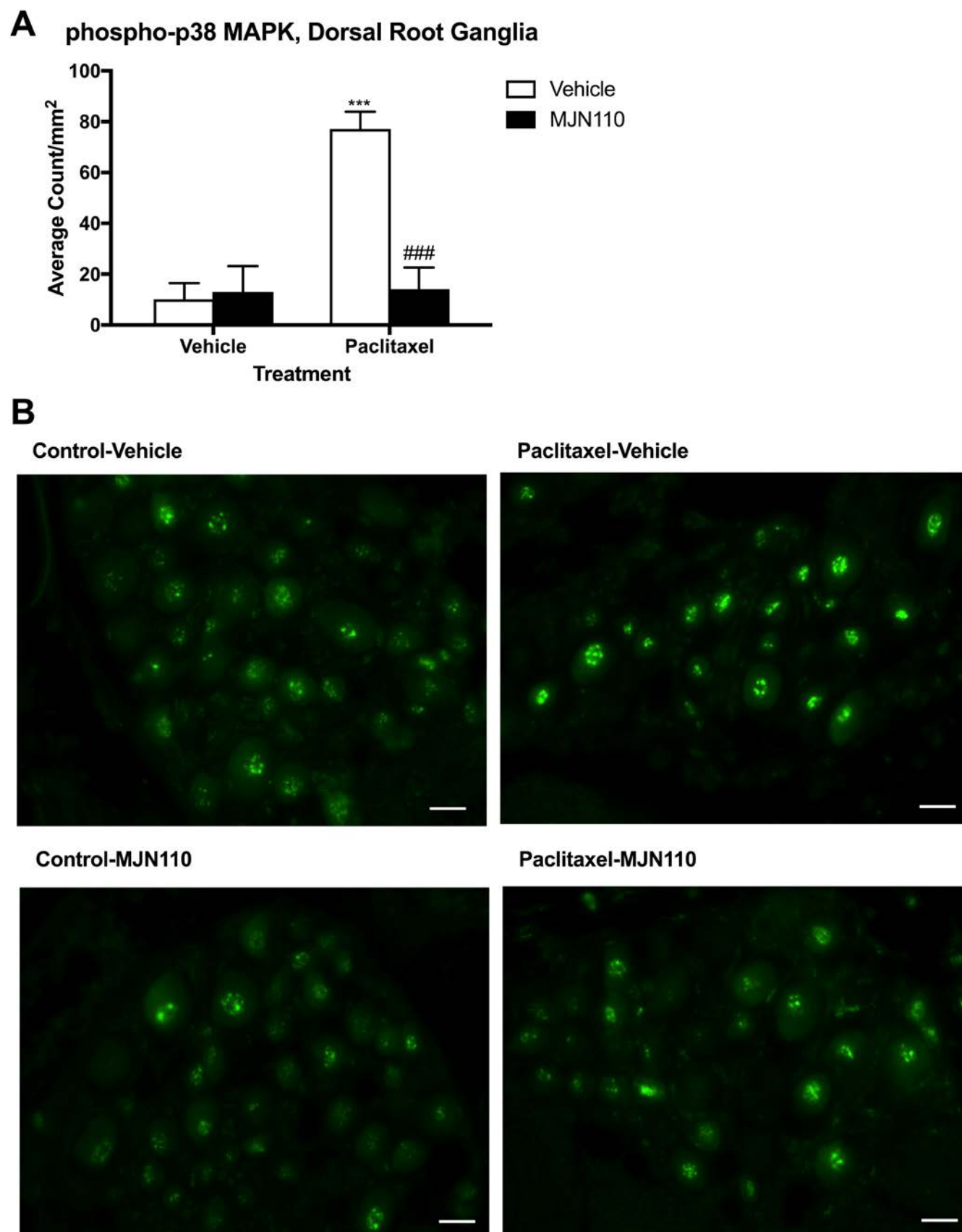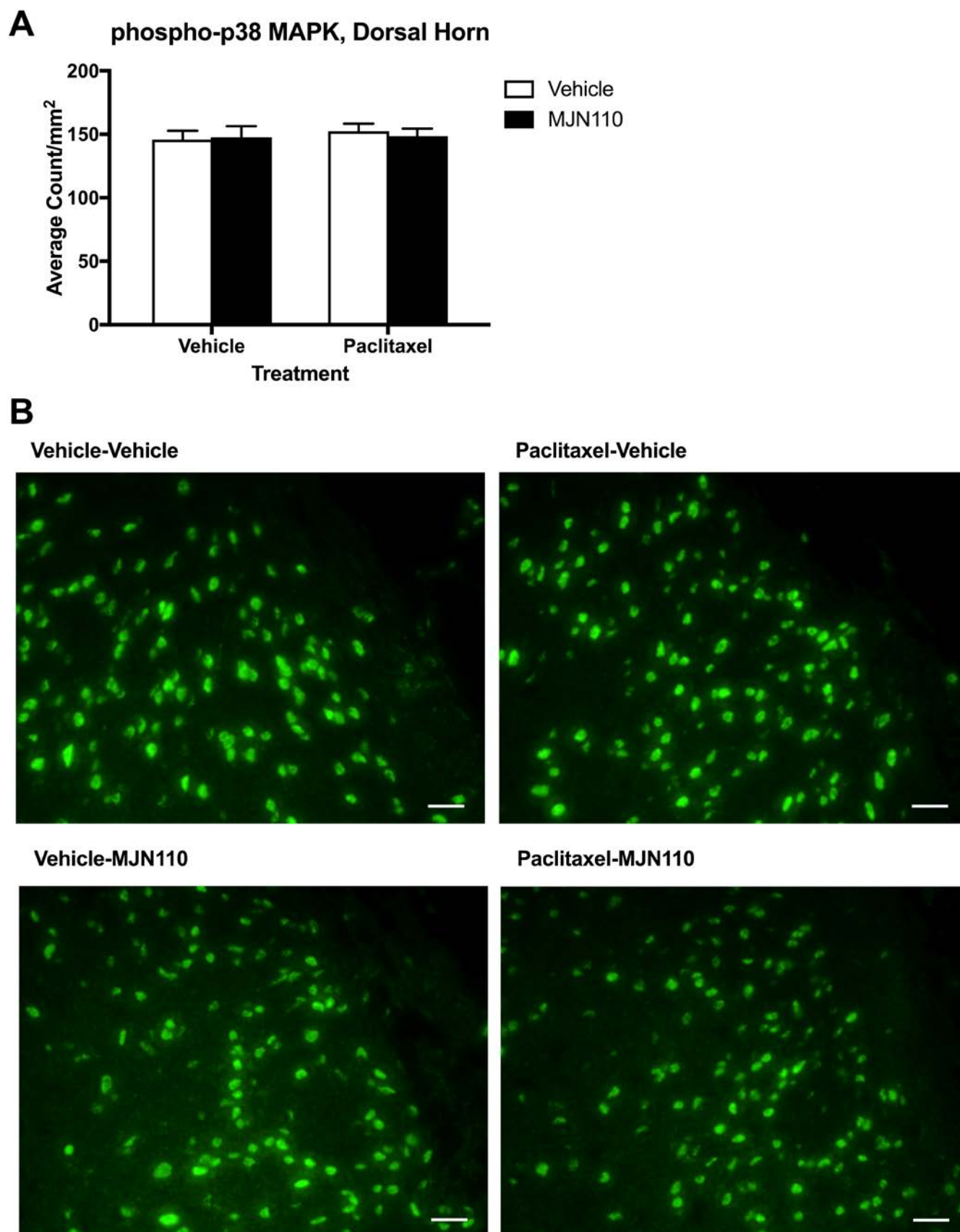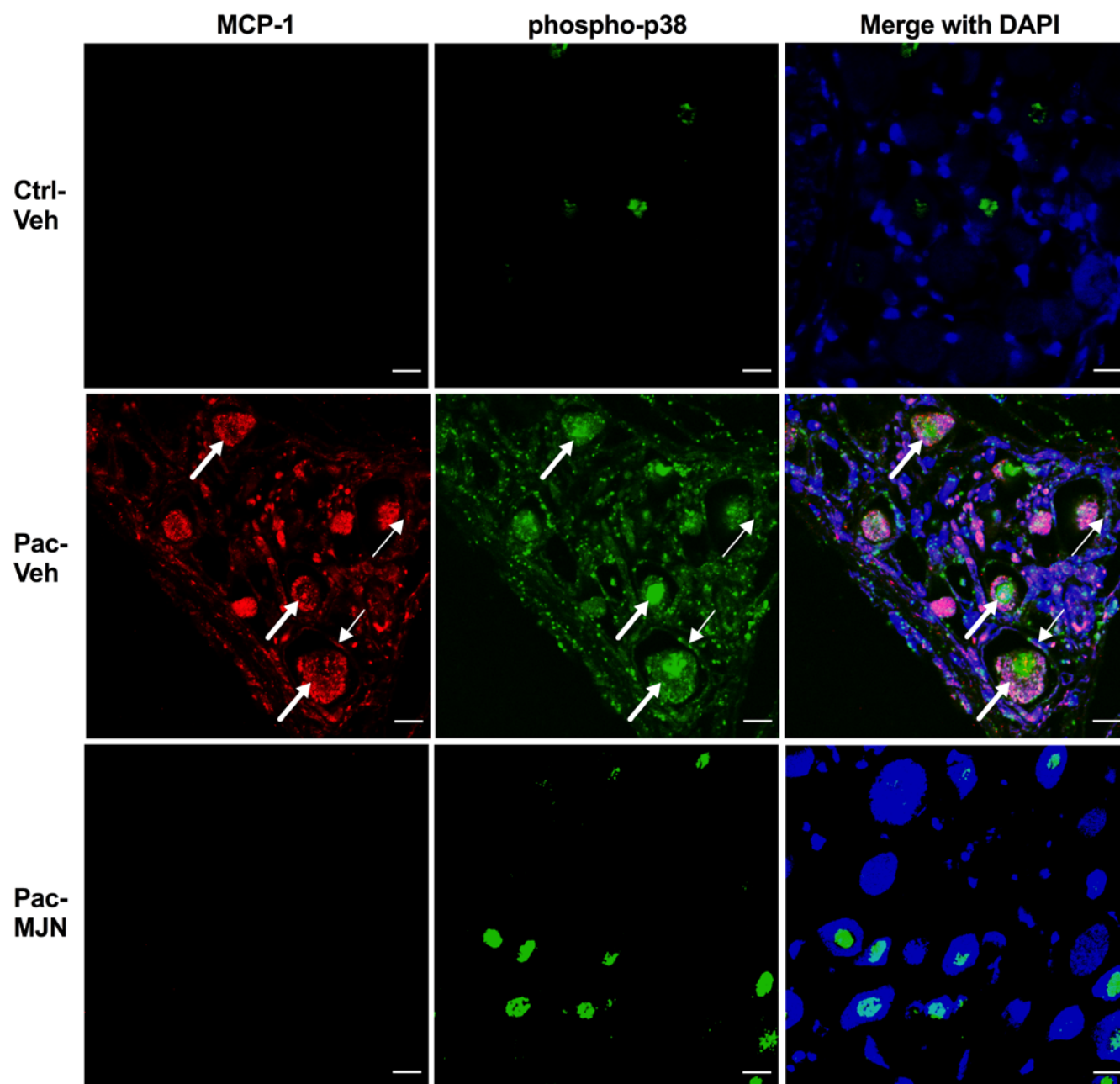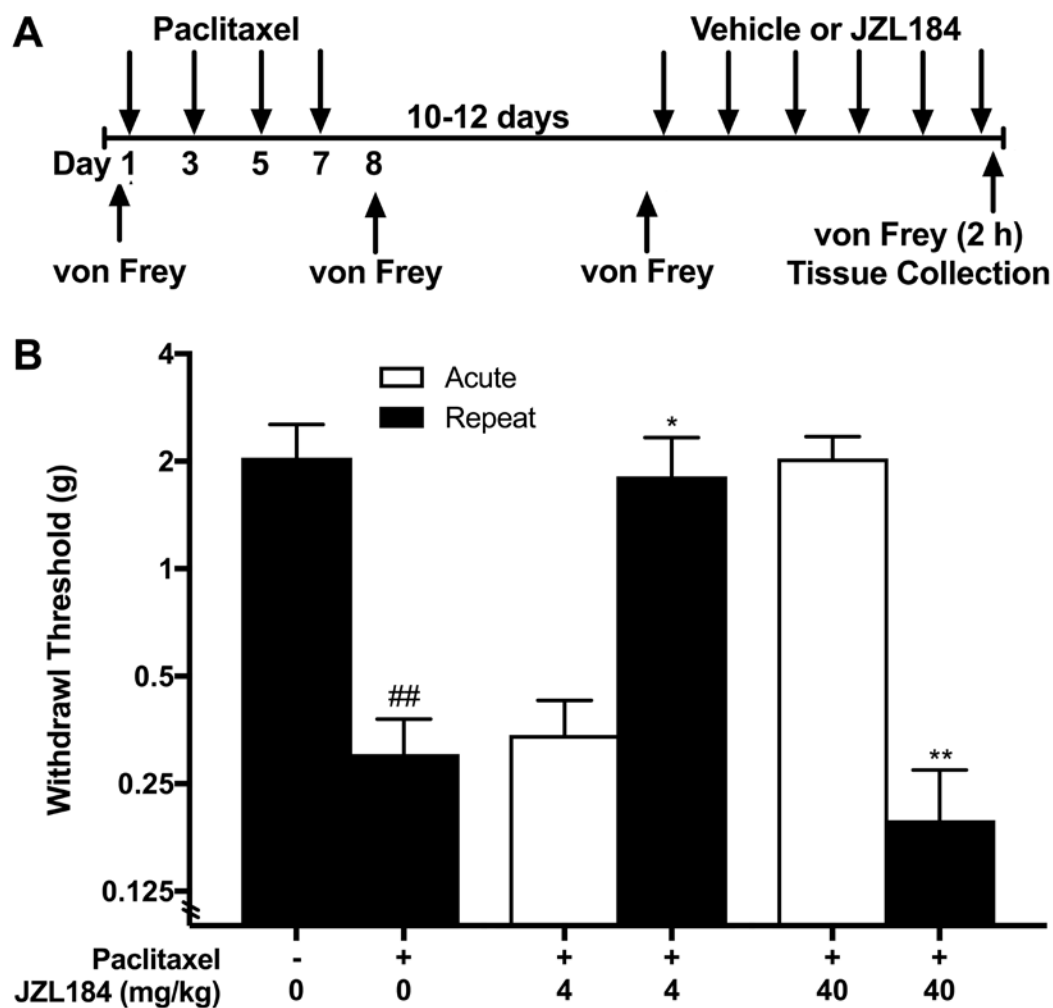
Figure 8
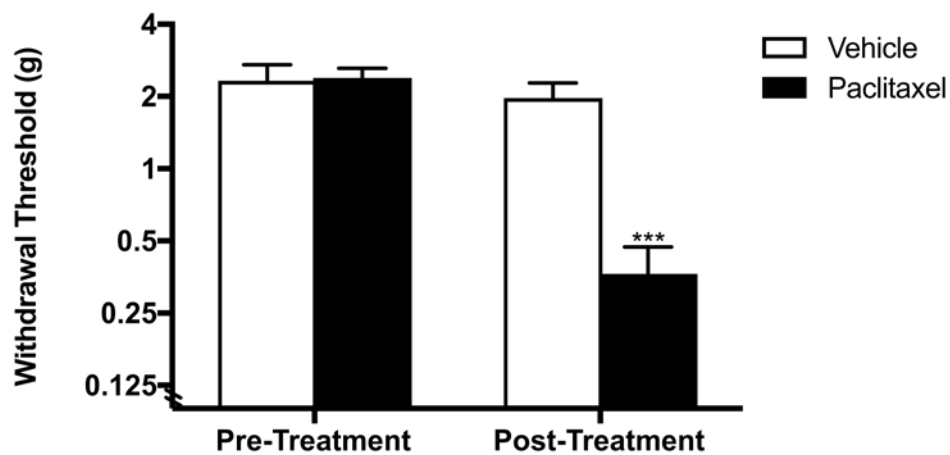
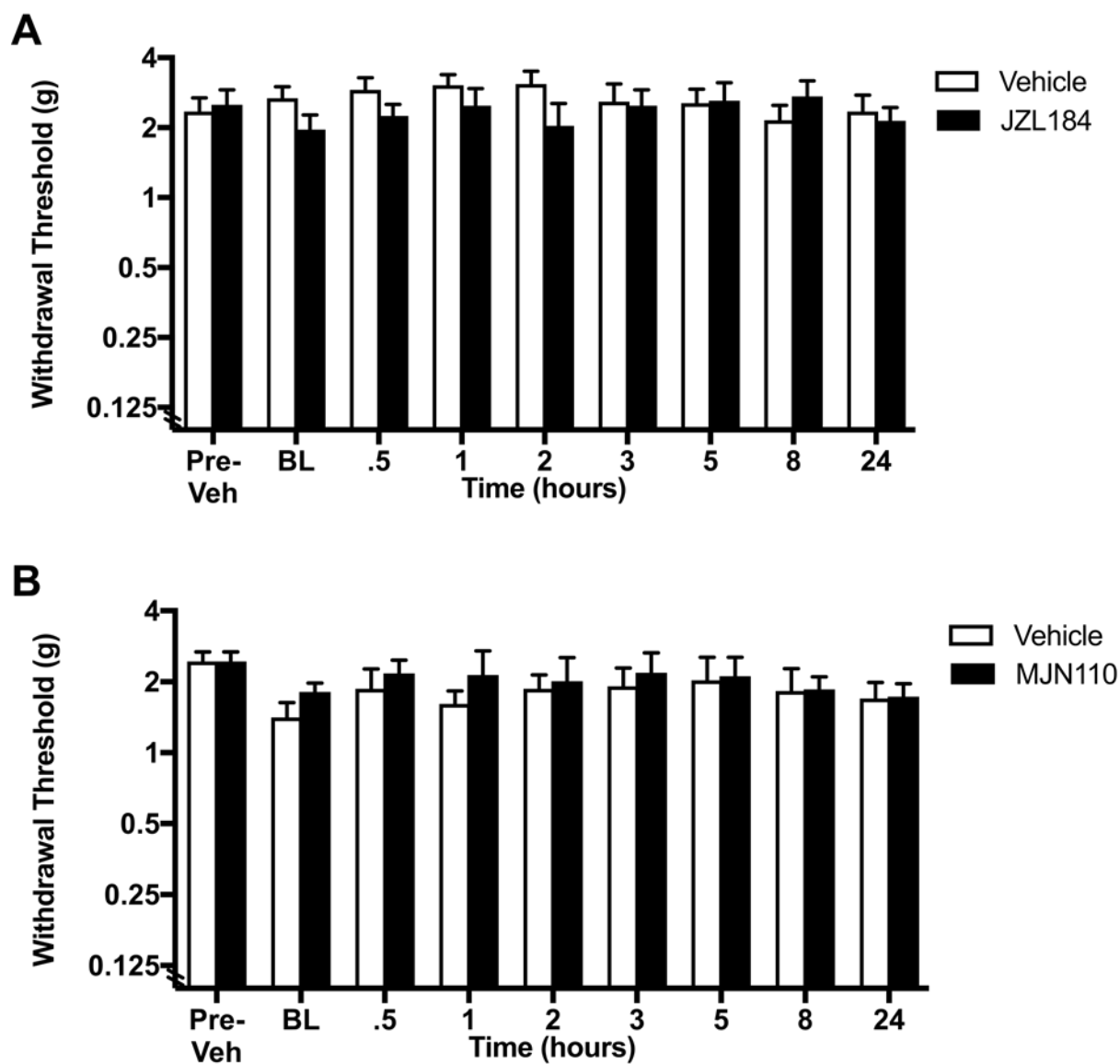Figure 9

Figure 10
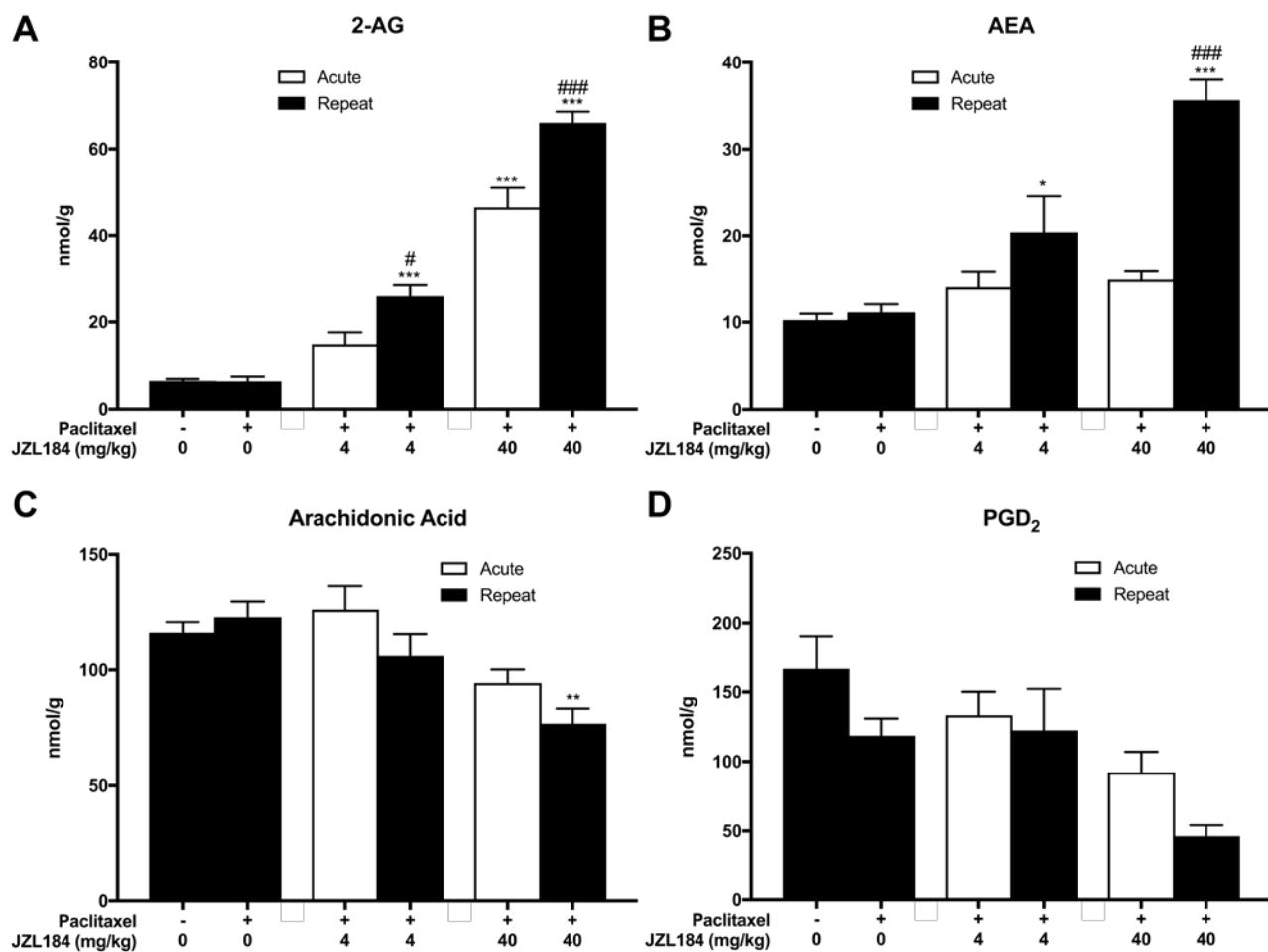
Figure 11
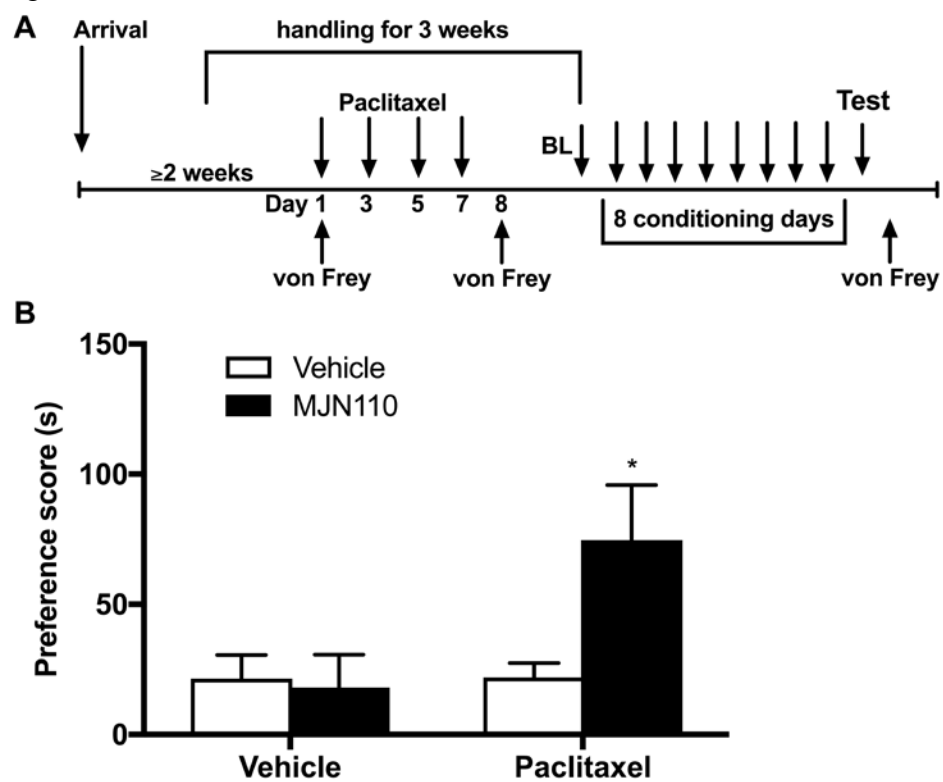
Figure 12
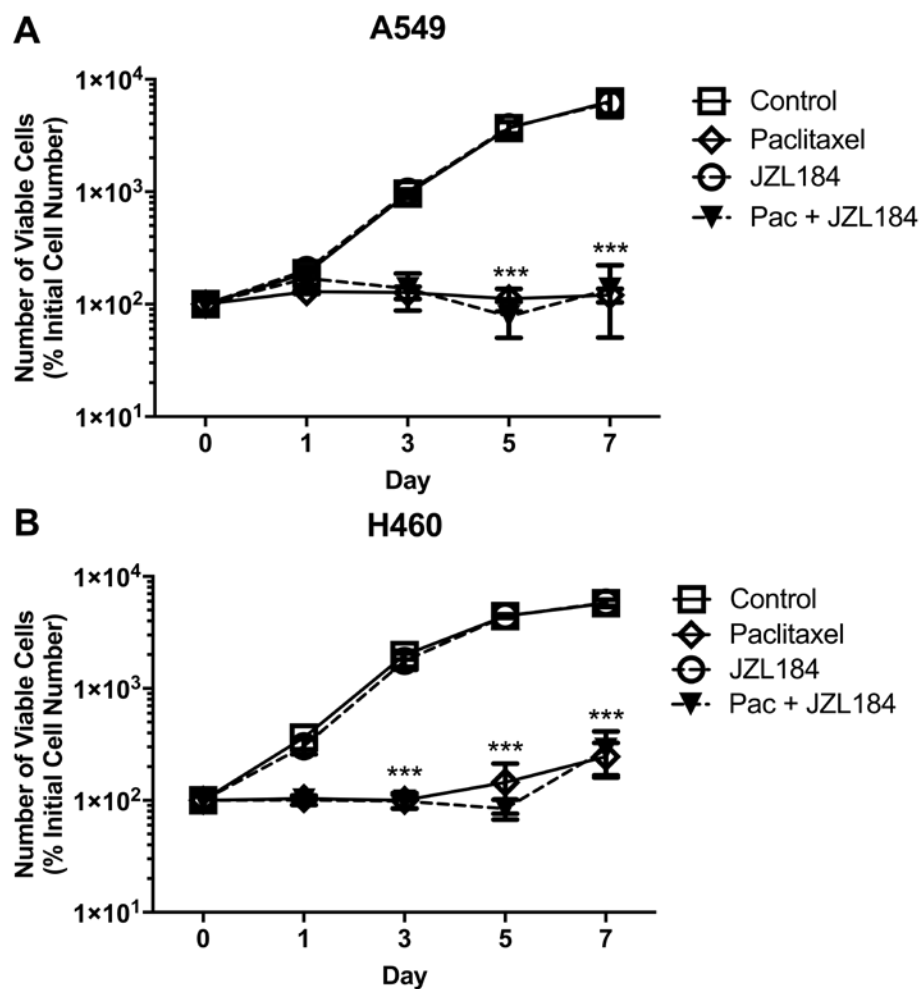
Figure 13

Supplemental Data

Monoacylglycerol lipase inhibitors reverse paclitaxel-induced nociceptive behavior and proinflammatory markers in a mouse model of chemotherapy-induced neuropathy

Zachary A Curry, Jenny L Wilkerson, Deniz Bagdas, S Lauren Kyte, Nipa Patel, Giulia Donvito, Mohammed A Mustafa, Justin L Poklis, Micah J Niphakis, Ku-Lung Hsu, Benjamin F Cravatt, David A Gewirtz, M Imad Damaj, Aron H Lichtman

Journal of Pharmacology and Experimental Therapeutics

Supplemental Figure 1. A cycle of paclitaxel induces a significant mechanical allodynia. Prior to treatment with paclitaxel or vehicle, mice were assessed for paw withdrawal using von Frey filaments. After testing, 8 mg/kg of paclitaxel (or equivalent volume of vehicle) was administered i.p. on alternate days for a total of four injections (cumulative dose: 32 mg/kg). On the day after the last injection, paw withdrawal thresholds were assessed. Data are reported as mean ± S.E.M., n = 7-8 mice/group. ***P<0.001 vs control (vehicle-treated) mice.

Supplemental Figure 2. MAGL inhibitors do alter paw withdrawal thresholds in control mice that did not receive paclitaxel. Neither (**A**) 40 mg/kg JZL184 nor (**B**) 5 mg/kg MJN110 altered paw withdrawal thresholds compared with vehicle. Pre-Veh= baseline prior to vehicle-treatment. BL = baseline prior to drug administration. Data are reported as mean ± S.E.M., n = 8 mice/group.
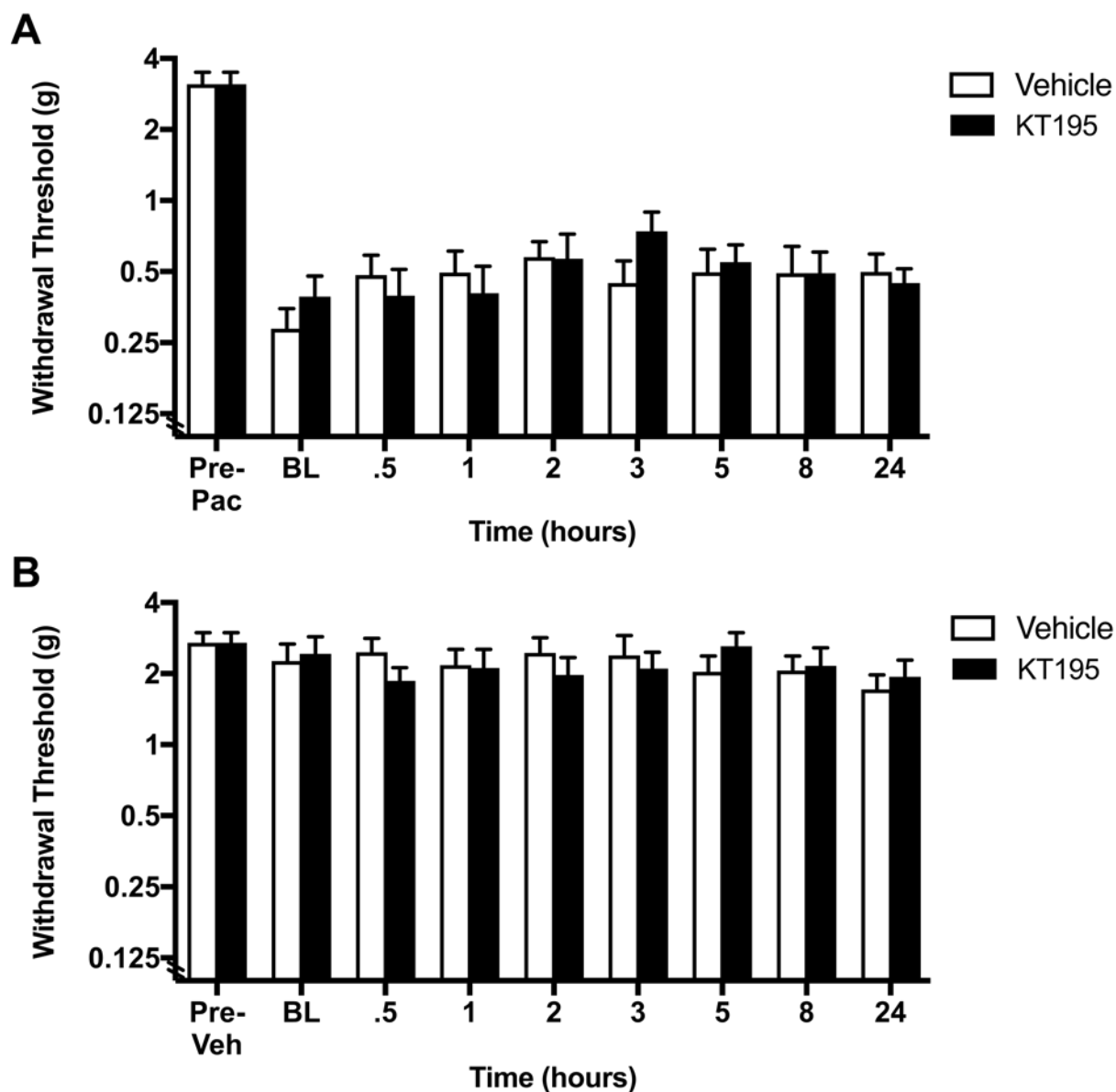
Supplemental Figure 3. The ABHD6 inhibitor KT195 (40 mg/kg) did not alter paw withdrawal thresholds in either (**A**) paclitaxel (pac)-treated or (**B**) vehicle (veh) control mice. BL = baseline prior to drug administration. Data are reported as mean ± S.E.M., $n = 8$ mice/group.
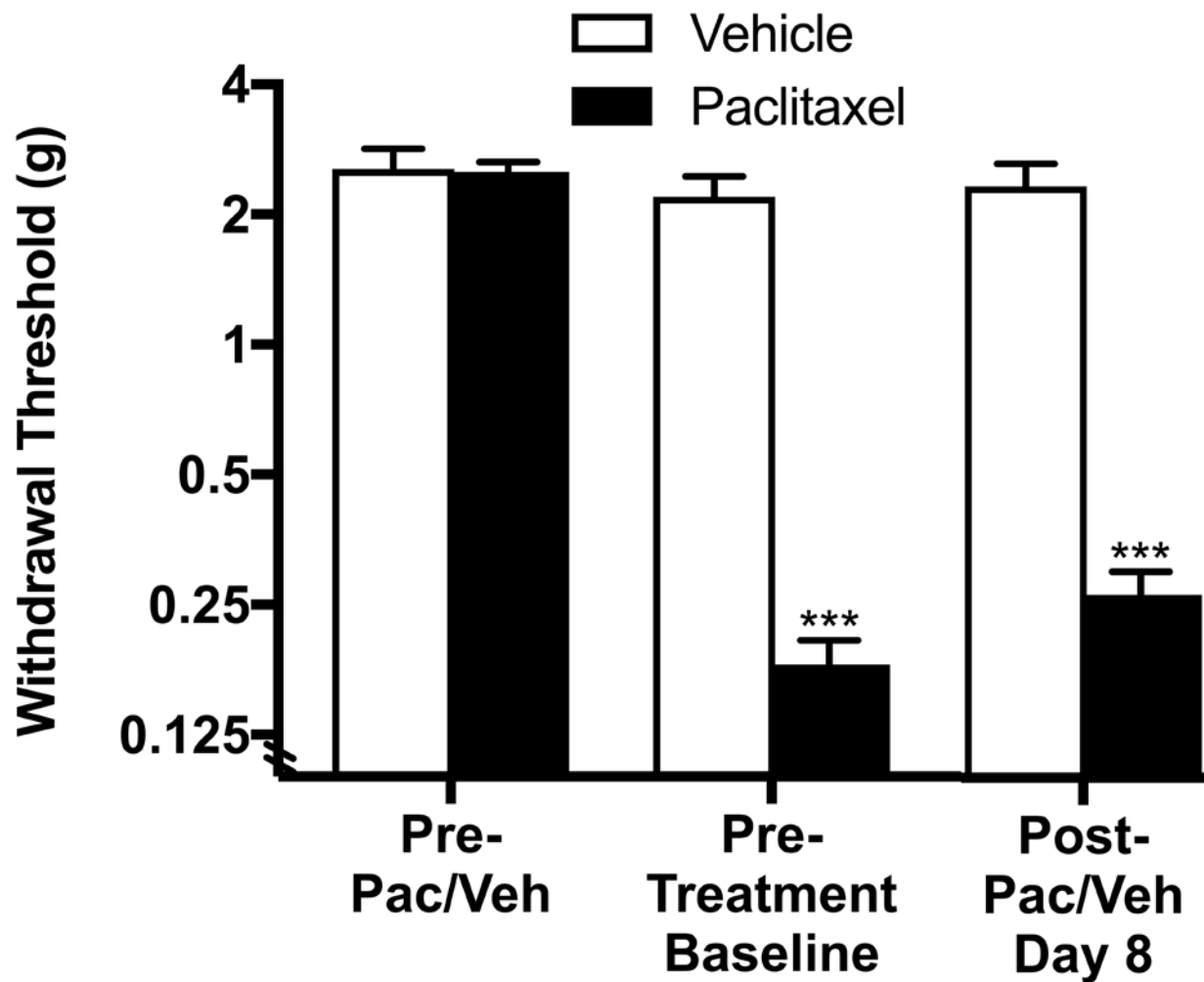
Supplemental Figure 4. Paclitaxel-treated mice from the conditioned place preference (CPP) experiment developed a significant mechanical allodynia compared to the control group that was not treated with paclitaxel. Allodynia was observed before commencing the first CPP sessions and following the conclusion of the experiment. Data are reported as mean ± S.E.M., n = 31-32 mice/group. ***P<0.001 vs vehicle control mice.